Design, Synthesis, Characterization and Evaluation of Anticancer Activity of Water-Soluble Half-sandwich Ruthenium (II) Arene Halido Complexes

Tanveer A. Khan,[a] Kishalay Bhar,[a] Ramalingam Thirumoorthi,[a] Tapta Kanchan Roy*[b] and Anuj K. Sharma*[a]

[a]*Department of Chemistry, School of Chemical Sciences and Pharmacy, Central University of Rajasthan, Bandarsindri, District Ajmer, Rajasthan, 305817, India.*

[b]*Department of Chemistry & Chemical Sciences, Central University of Jammu, Rahya-Suchani (Bagla), District-Samba, Jammu-181143, (J&K) India.*

Supporting information

Contents

		298 K.
30.	**Figure S29.**	UV-Visible absorption spectra of **2** (26.66 μM) recorded in DMSO after 0, 2, 12, 24 and 48 h at 298 K.
31.	**Figure S30.**	UV-Visible absorption spectra of **3** (26.66 μM) recorded in DMSO after 0, 2, 12, 24 and 48 h at 298 K.
32.	**Figure S31.**	^{1}H-NMR spectrum of **1** recorded in DMSO-d_6 after 0, 0.5, 2, 6, 24 and 48 h at 298 K.
33.	**Figure S32.**	^{1}H-NMR spectrum of **2** recorded in DMSO-d_6 after 0 h, 10 min., 0.5 h, 2 h, 6 h, 24 h and 48 h at 298 K.
34.	**Figure S33.**	^{1}H-NMR spectrum of **3** recorded in DMSO-d_6 after 0, 0.5, 2, 6, 24 and 48 h at 298 K.
35.	**Figure S34.**	UV-Visible absorption spectra of **L_1**, **L_2**, **L_3**and Ru(p-cymene)dimer (26.66 μM) recorded in DMSO at 298 K.
36.	**Figure S35.**	UV-Visible absorption spectra of **L_1** (26.66 μM) recorded in DMSO after 0, 12, 24 and 48 h at 298 K.
37.	**Figure S36.**	UV-Visible absorption spectra of **L_2** (26.66 μM) recorded in DMSO after 0, 12, 24 and 48 h at 298 K.
38.	**Figure S37.**	UV-Visible absorption spectra of **L_3** (26.66 μM) recorded in DMSO after 0, 12, 24 and 48 h at 298 K.
39.	**Figure S38.**	UV-Visible absorption spectra of Ru(p-cymene)dimer (26.66 μM) recorded in DMSO after 0, 12, 24 and 48 h at 298 K.
40.	**Figure S39.**	UV-Visible absorption spectra of Ru(p-cymene)dimer (26.66 μM) recorded in PBS (pH = 7.4) after 0, 12, 24 and 48 h at 298 K.
41.	**Figure S40.**	Demonstrating intermolecular π-π stacking interactions for **1**; [Hydrogen atoms and solvent molecules omitted for clarity].
42.	**Figure S41.**	Showing C-H···Cl and N-H···Cl hydrogen bonded network in crystal structure of **1**.
43.	**Table S1.**	Selected bond distances and bond angles (Å, º) observed in crystal structure of **1**.
44.	**Table S2.**	π···π interaction parameters (Å, º) associated with crystal structure of **1**.
45.	**Table S3.**	Hydrogen bond parameters (Å, º) associated with crystal structure of **1**.
46.	**Figure S42.**	Cyclic voltammograms of **1** (1 mM) solution in CH_3CN with 0.1 M $[nBu_4N][ClO_4]$ at scan rates: 100 mV s^{-1}, 200 mV s^{-1}, 500 mV s^{-1}, 1000 mV s^{-1} at room temperature (Range: 0.5 to 1.5 V).
47.	**Figure S43.**	Cyclic voltammograms of **2** (1 mM) solution in CH_3CN with 0.1 M $[nBu_4N][ClO_4]$ at scan rates: 100 mV s^{-1}, 200 mV s^{-1}, 500 mV s^{-1}, 1000 mV s^{-1} at room temperature (Range: 0.5 to 1.95 V and 0.5 to 1.5 V).
48.	**Figure S44.**	Cyclic voltammograms of **3** (1 mM) solution in CH_3CN with 0.1 M $[nBu_4N][ClO_4]$ at scan rates: 100 mV s^{-1}, 200 mV s^{-1}, 500 mV s^{-1}, 1000 mV s^{-1} at room temperature (Range: 0.5 to 2.0 V and 0.5 to 1.5 V).
49.	**Figure S45A.**	DFT optimized structures of the global minima (with and without solvent) with frontier MOs of **1**.
50.	**Figure S45B.**	DFT optimized structures of the global minima (with and without solvent) with frontier MOs of **2**.
51.	**Figure S46.**	Molecular docked model of **1** (right column) and **2** (left column) with B-DNA optimized at PM6 method.
52.	**Table S4.**	Selected bond lengths (Å) and bond angles (˚) of **1** in DFT optimized structures (at B3LYP/6-31G(d,p)/LanL2DZ level of theory)with and without solvent.
53.	**Table S5.**	Selected bond lengths (Å) and bond angles (˚) of **2** in DFT optimized structures (at B3LYP/6-31G(d,p)/LanL2DZ level of theory) of with and without solvent for four different conformers **A, B, C** and **D**.
54.	**Figure S47.**	UV-Visible absorption titration spectra of **2** (10 μM; Milli-Q water) with the addition of varying concentrations of CT-DNA (0-15 μM; $T_{10}E_1$ buffer, pH ~ 7.6) at 298 K.
55.	**Figure S48.**	UV-Visible absorption titration spectra of **3** (10 μM; Milli-Q water) with the addition of varying concentrations of CT-DNA (0-15 μM; $T_{10}E_1$ buffer, pH ~ 7.6) at 298 K.
56.	**Figure S49.**	Plot for the calculation of equilibrium binding constant (K_b) associated with the titration of **2** and CT-DNA at 298 K.
57.	**Figure S50.**	Plot for the calculation of equilibrium binding constant (K_b) associated with the titration of **3** and CT-DNA at 298 K.
58.	**Figure S51.**	Plot to the model of Bard and Thorp associated with the titration of **2** and CT-DNA at 298 K.
59.	**Figure S52.**	Plot to the model of Bard and Thorp associated with the titration of **3** and CT-DNA at 298 K.
60.	**Table S6.**	Molar absorptivity changes (Δϵ) for UV-Visible absorption studies of DNA binding with complex **1-3**.

61.	**Figure S53.**	UV-Visible absorption titration spectra of $\mathbf{L_1}$ (25 μM; DMSO:Water (5:100 v/v)) with the addition of varying concentrations of CT-DNA (0-4.3 x 10^{-7} M; $T_{10}E_1$ buffer, pH ~ 7.6) at 298 K.
62.	**Figure S54.**	UV-Visible absorption titration spectra of $\mathbf{L_2}$ (25 μM; DMSO:Water (5:100 v/v)) with the addition of varying concentrations of CT-DNA (0-4.3 x 10^{-7} M; $T_{10}E_1$ buffer, pH ~ 7.6) at 298 K.
63.	**Figure S55.**	UV-Visible absorption titration spectra of $\mathbf{L_3}$ (25 μM; DMSO:Water (5:100 v/v)) with the addition of varying concentrations of CT-DNA (0-4.3 x 10^{-7} M; $T_{10}E_1$ buffer, pH ~ 7.6) at 298 K.
64.	**Figure S56.**	Plot for the calculation of equilibrium binding constant (K_b) associated with the titration of $\mathbf{L_1}$ and CT-DNA at 298 K.
65.	**Figure S57.**	Plot for the calculation of equilibrium binding constant (K_b) associated with the titration of $\mathbf{L_2}$ and CT-DNA at 298 K.
66.	**Figure S58.**	Plot for the calculation of equilibrium binding constant (K_b) associated with the titration of $\mathbf{L_3}$ and CT-DNA at 298 K.
67.	**Figure S59.**	Plot to the model of Bard and Thorp associated with the titration of $\mathbf{L_1}$ and CT-DNA at 298 K.
68.	**Figure S60.**	Plot to the model of Bard and Thorp associated with the titration of $\mathbf{L_2}$ and CT-DNA at 298 K.
69.	**Figure S61.**	Plot to the model of Bard and Thorp associated with the titration of $\mathbf{L_3}$ and CT-DNA at 298 K.
70.	**Table S7.**	Data for UV-Visible absorption studies for DNA binding with ligand $\mathbf{L_1}$-$\mathbf{L_3}$.
71.	**Figure S62.**	Molecular fluorescence emission profile associated with titration of EthBr-DNA (35 μM; $T_{10}E_1$ buffer, pH ~ 7.6; $\lambda_{ex.}$ 480 nm; $\lambda_{em.}$ 597 nm) with the addition of varying concentrations of **2** (0-360 μM; Milli-Q water) at 298 K.
72.	**Figure S63.**	Molecular fluorescence emission profile associated with titration of EthBr-DNA (35 μM; $T_{10}E_1$ buffer, pH ~ 7.6; $\lambda_{ex.}$ 480 nm; $\lambda_{em.}$ 597 nm) with the addition of varying concentrations of **3** (0-270 μM; Milli-Q water) at 298 K.
73.	**Figure S64.**	Stern-Volmer plot for the calculation of quenching constant (K_{SV}) associated with the titration of EthBr-DNA and **1** at 298 K.
74.	**Figure S65.**	Stern-Volmer plot for the calculation of quenching constant (K_{SV}) associated with the titration of EthBr-DNA and **2** at 298 K.
75.	**Figure S66.**	Stern-Volmer plot for the calculation of quenching constant (K_{SV}) associated with the titration of EthBr-DNA and **3** at 298 K.
76.	**Figure S67.**	Scatchard plot for the calculation of association constant (K_a) related with the interaction of EthBr-DNA and **1** at 298 K.
77.	**Figure S68.**	Scatchard plot for the calculation of association constant (K_a) related with the interaction of EthBr-DNA and **2** at 298 K.
78.	**Figure S69.**	Scatchard plot for the calculation of association constant (K_a) related with the interaction of EthBr-DNA and **3** at 298 K.
79.	**Figure S70.**	Molecular fluorescence emission profile associated with titration of EthBr-DNA (35 μM; $T_{10}E_1$ buffer, pH ~ 7.6; $\lambda_{ex.}$ 480 nm; $\lambda_{em.}$ 597 nm) with the addition of varying concentrations of $\mathbf{L_1}$ (0-7.24 x 10^{-4} M; DMSO:Water (5:100 v/v)) at 298 K.
80.	**Figure S71.**	Molecular fluorescence emission profile associated with titration of EthBr-DNA (35 μM; $T_{10}E_1$ buffer, pH ~ 7.6; $\lambda_{ex.}$ 480 nm; $\lambda_{em.}$ 597 nm) with the addition of varying concentrations of $\mathbf{L_3}$ (0-4.42 x 10^{-4} M ; DMSO:Water (5:100 v/v)) at 298 K.
81.	**Figure S72.**	Molecular fluorescence emission profile associated with titration of EthBr-DNA (35 μM; $T_{10}E_1$ buffer, pH ~ 7.6; $\lambda_{ex.}$ 480 nm; $\lambda_{em.}$ 597 nm) with the addition of varying concentrations of Ru(p-cymene)dimer (0-6.03 x 10^{-4} M; Milli-Q water) at 298 K.
82.	**Figure S73.**	Stern-Volmer plot for the calculation of quenching constant (K_{SV}) associated with the titration of EthBr-DNA and $\mathbf{L_1}$ at 298 K.
83.	**Figure S74.**	Stern-Volmer plot for the calculation of quenching constant (K_{SV}) associated with the titration of EthBr-DNA and $\mathbf{L_3}$ at 298 K.
84.	**Figure S75.**	Stern-Volmer plot for the calculation of quenching constant (K_{SV}) associated with the titration of EthBr-DNA and Ru(p-cymene)dimer at 298 K.
85.	**Figure S76.**	Scatchard plot for the calculation of association constant (K_a) related with the interaction of EthBr-DNA and $\mathbf{L_1}$ at 298 K.
86.	**Figure S77.**	Scatchard plot for the calculation of association constant (K_a) related with the interaction of EthBr-DNA and $\mathbf{L_3}$ at 298 K.
87.	**Figure S78.**	Scatchard plot for the calculation of association constant (K_a) related with the interaction of EthBr-DNA and Ru(p-cymene)dimer at 298 K.
88.	**Table S8.**	Data for emission spectroscopic studies for DNA binding with ligand $\mathbf{L_1}$, $\mathbf{L_3}$ and Ru(p-cymene)dimer.
89.	**Figure S79.**	Molecular fluorescence emission profile associated with titration of BSA (0.15 μM; PBS, pH ~ 7.4; $\lambda_{ex.}$ 280 nm; $\lambda_{em.}$ 344 nm) with the addition of varying concentrations of **2** (0-16 μM; PBS, pH ~ 7.4) at 298 K.

90.	**Figure S80.**	Molecular fluorescence emission profile associated with titration of BSA (0.15 μM; PBS, pH ~ 7.4; $\lambda_{ex.}$ 280 nm; $\lambda_{em.}$ 344 nm) with the addition of varying concentrations of **3** (0-16 μM; PBS, pH ~ 7.4) at 298 K.
91.	**Figure S81.**	Molecular fluorescence emission profile associated with titration of BSA (0.15 μM; PBS, pH ~ 7.4; $\lambda_{ex.}$ 280 nm; $\lambda_{em.}$ 344 nm) with the addition of varying concentrations of Ru(p-cymene)dimer (0-16 μM; PBS, pH ~ 7.4) at 298 K.
92.	**Figure S82.**	Stern-Volmer plot for the calculation of quenching constant (K_{SV}) associated with the interaction of BSA and **1** at 298 K.
93.	**Figure S83.**	Stern-Volmer plot for the calculation of quenching constant (K_{SV}) associated with the interaction of BSA and **2** at 298 K.
94.	**Figure S84.**	Stern-Volmer plot for the calculation of quenching constant (K_{SV}) associated with the interaction of BSA and **3** at 298 K.
95.	**Figure S85.**	Stern-Volmer plot for the calculation of quenching constant (K_{SV}) associated with the interaction of BSA and Ru(p-cymene)dimer at 298 K.
96.	**Figure S86.**	Scatchard plot for the calculation of binding constant (K_b) associated with the interaction of BSA and **1** at 298 K.
97.	**Figure S87.**	Scatchard plot for the calculation of binding constant (K_b) associated with the interaction of BSA and **2** at 298 K.
98.	**Figure S88.**	Scatchard plot for the calculation of binding constant (K_b) associated with the interaction of BSA and **3** at 298 K.
99.	**Figure S89.**	Scatchard plot for the calculation of binding constant (K_b) associated with the interaction of BSA and Ru(p-cymene)dimer at 298 K.
100.	**Table S9.**	Data for emission spectroscopic studies for BSA interaction with Ru(p-cymene)dimer.
101.	**Figure S90.**	UV-Visible absorption spectra of BSA (10 μM; PBS, pH ~ 7.4) in presence of **1-3** (10 μM; PBS, pH ~ 7.4) at 298 K.
102.	**Figure S91.**	UV-Visible absorption spectra of BSA (10 μM; PBS, pH ~ 7.4) in presence of **L_1, L_2, L_3** and Ru(p-cymene)dimer (10 μM; DMSO:Water (5:100 v/v)) at 298 K.
103.	**Figure S92.**	Synchronous fluorescence emission profile associated with titration of BSA (0.15 μM; PBS, pH ~ 7.4) with the addition of varying concentrations of **2** (0-16 μM; PBS, pH ~ 7.4) at the wavelength difference of $\Delta\lambda$ = 60 nm.
104.	**Figure S93.**	Synchronous fluorescence emission profile associated with titration of BSA (0.15 μM; PBS, pH ~ 7.4) with the addition of varying concentrations of **3** (0-16 μM; PBS, pH ~ 7.4) at the wavelength difference of $\Delta\lambda$ = 60 nm.
105.	**Figure S94.**	Synchronous fluorescence emission profile associated with titration of BSA (0.15 μM; PBS, pH ~ 7.4) with the addition of varying concentrations of Ru(p-cymene)dimer (0-16 μM; PBS, pH ~ 7.4) at the wavelength difference of $\Delta\lambda$ = 60 nm.
106.	**Figure S95.**	Synchronous fluorescence emission profile associated with titration of BSA (0.15 μM; PBS, pH ~ 7.4) with the addition of varying concentrations of **2** (0-16 μM; PBS, pH ~ 7.4) at the wavelength difference of $\Delta\lambda$ = 15 nm.
107.	**Figure S96.**	Synchronous fluorescence emission profile associated with titration of BSA (0.15 μM; PBS, pH ~ 7.4) with the addition of varying concentrations of **3** (0-16 μM; PBS, pH ~ 7.4) at the wavelength difference of $\Delta\lambda$ = 15 nm.
108.	**Figure S97.**	Synchronous fluorescence emission profile associated with titration of BSA (0.15 μM; PBS, pH ~ 7.4) with the addition of varying concentrations of Ru(p-cymene)dimer (0-16 μM; PBS, pH ~ 7.4) at the wavelength difference of $\Delta\lambda$ = 15 nm.
109.	**Figure S98.**	*In vitro* cytotoxicity of Ru precursor complex (a), **L_1** (b), **L_2** (c), **L_3** (d), complex **1** (e), complex **2** (f) and complex **3** (g) against MCF-7 cell lines measured by MTT assay after 48 h.
110.	**Figure S99.**	*In vitro* calculated IC_{50} values of Ru precursor complex (a), **L_1** (b), **L_2** (c), **L_3** (d), complex **1** (e), complex **2** (f) and complex **3** (g) against MCF-7 cell lines measured by MTT assay after 48 h.

CHNS REPORT

Method filename: C:\CHNS\Method\23-02-2018-test.mth
Method name: 23-02-2018-test
Printed: 03-01-2018 19:39
Elemental Analyser method:
Sampler method:
Sample ID: AS-TAK-35
Analysis type: UnkNown
Chromatogram filename: C:\CHNS\Method\AS-TAK-35-23-02-18.DAT
Calibration method: K Factors
Sample weight: 1.012

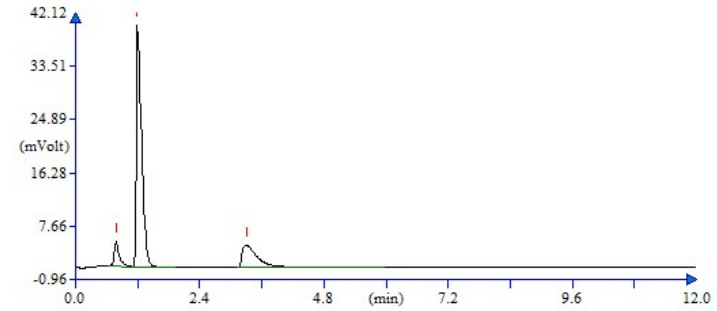

Component Name	Retention Time (min)	Area (.1*uV*sec)	Element %
Nitrogen	0.775	279960	7.252
Carbon	1.192	2717639	54.521
Hydrogen	3.300	745545	4.707
		3743143	66.481

Figure S1. Data and graph obtained from elemental analysis of **1**.

CHNS REPORT

Method filename: C:\CHNS\Method\23-02-2018-test.mth
Method name: 23-02-2018-test
Printed: 03-06-2018 19:24
Elemental Analyser method:
Sampler method:
Sample ID: AS-TAK-64
Analysis type: UnkNown
Chromatogram filename: C:\CHNS\Method\AS-TAK-64-24-02-18.DAT
Calibration method: K Factors
Sample weight: 1.303

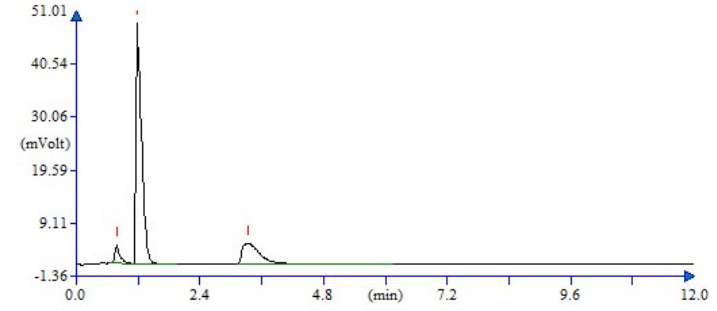

Component Name	Retention Time (min)	Area (.1*uV*sec)	Element %
Nitrogen	0.783	250178	4.263
Carbon	1.175	3440532	53.609
Hydrogen	3.325	1008916	4.959
		4699626	62.830

Figure S2. Data and graph obtained from elemental analysis of **2**.

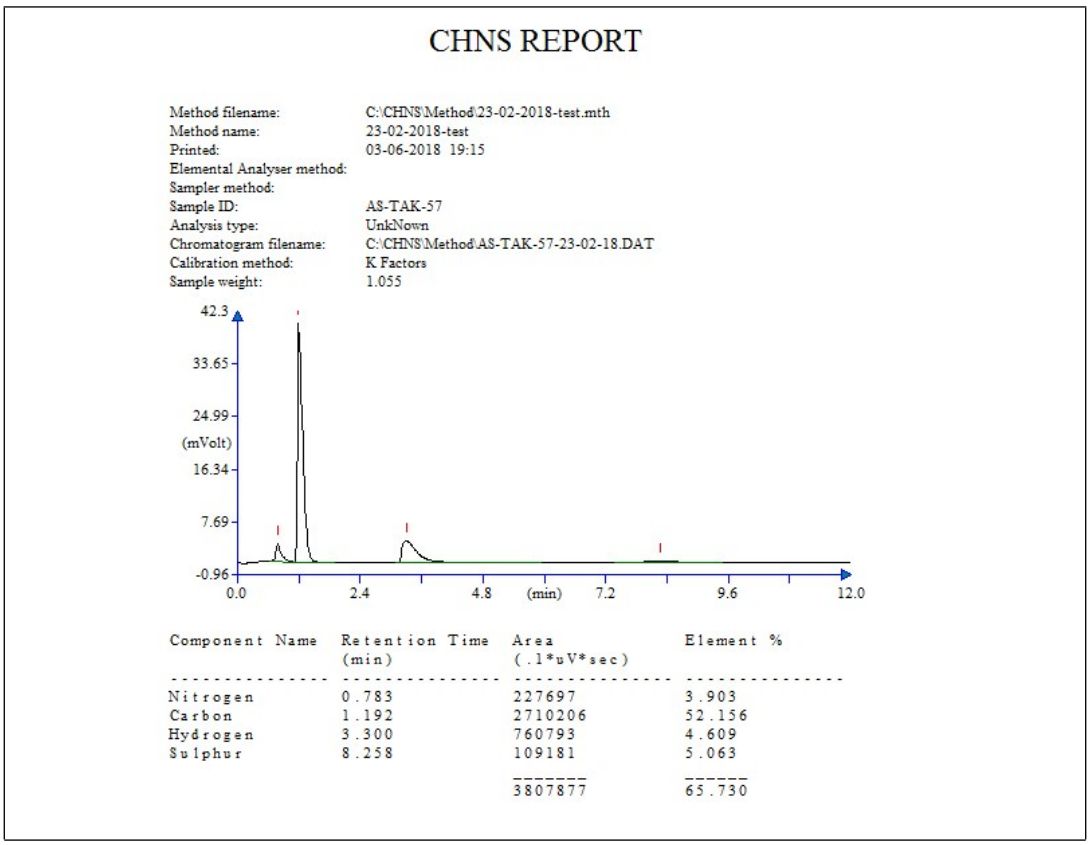

Figure S3. Data and graph obtained from elemental analysis of **3**.

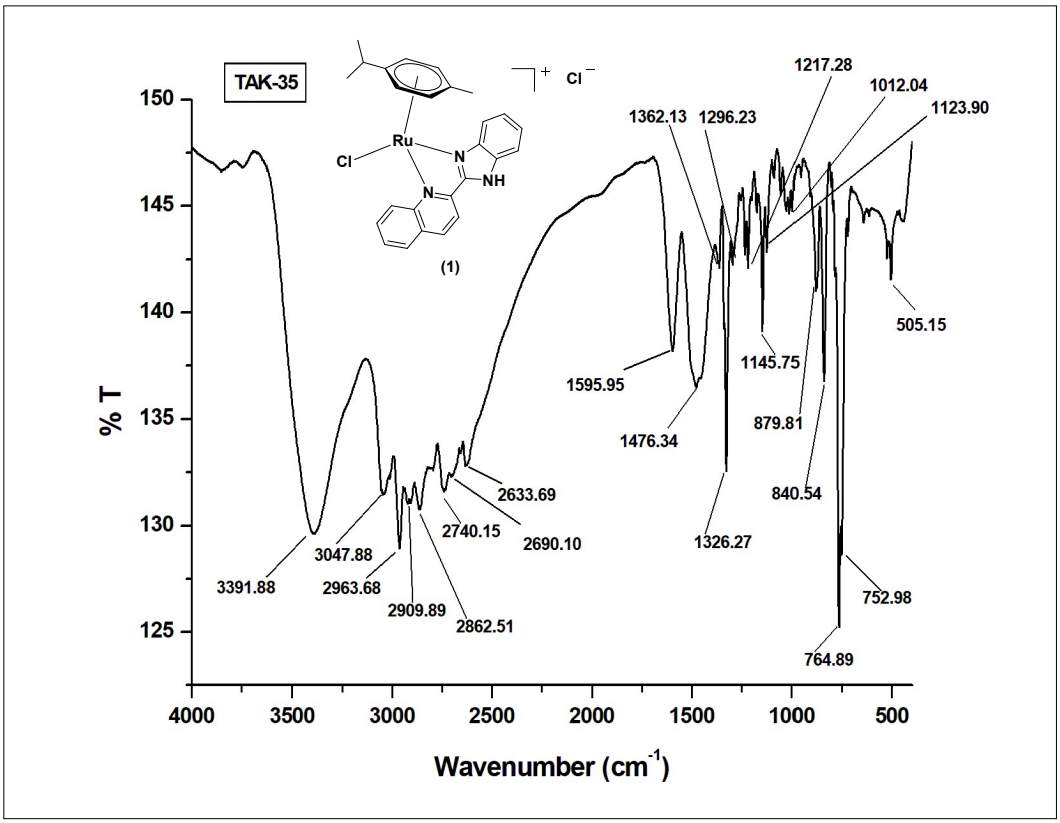

Figure S4. IR spectrum of **1** recorded using KBr disc technique.

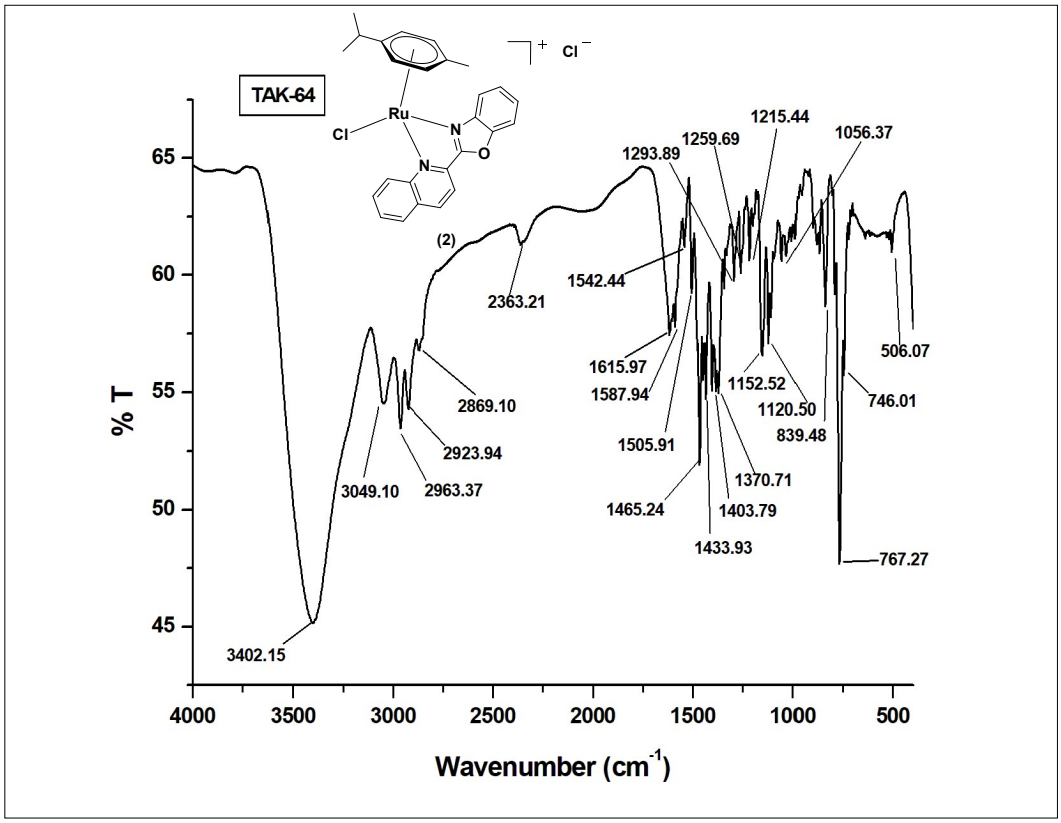

Figure S5. IR spectrum of **2** recorded using KBr disc technique.

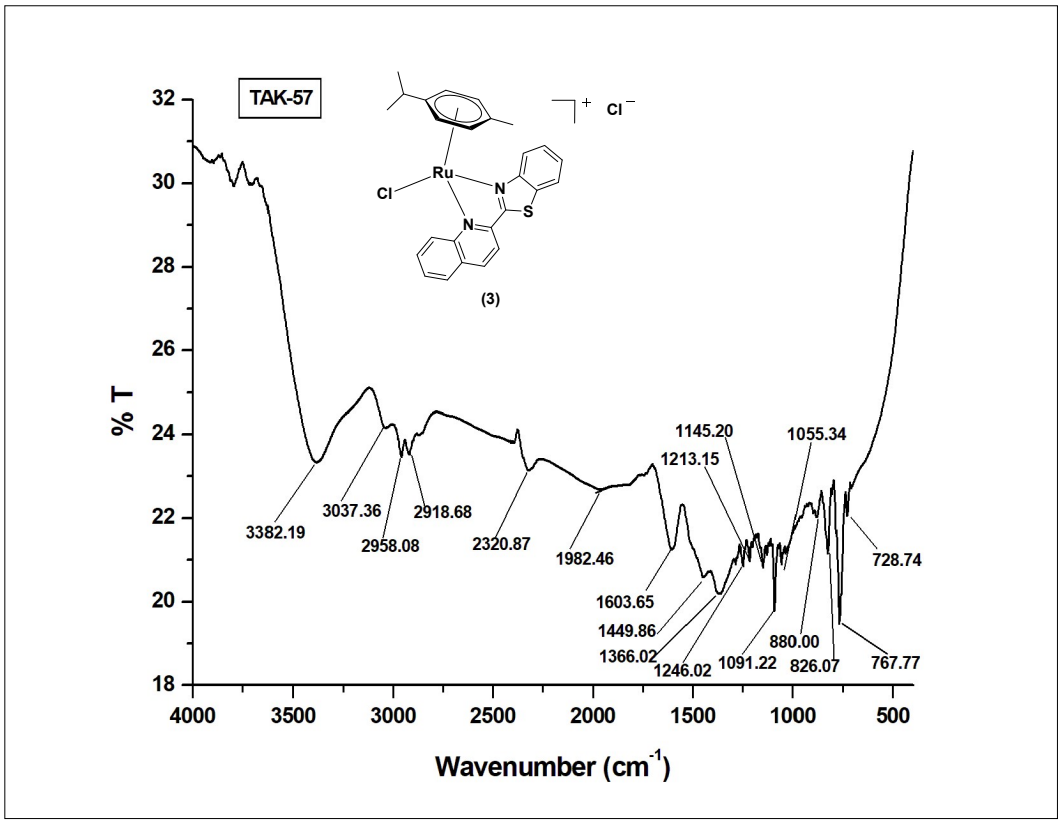

Figure S6. IR spectrum of **3** recorded using KBr disc technique.

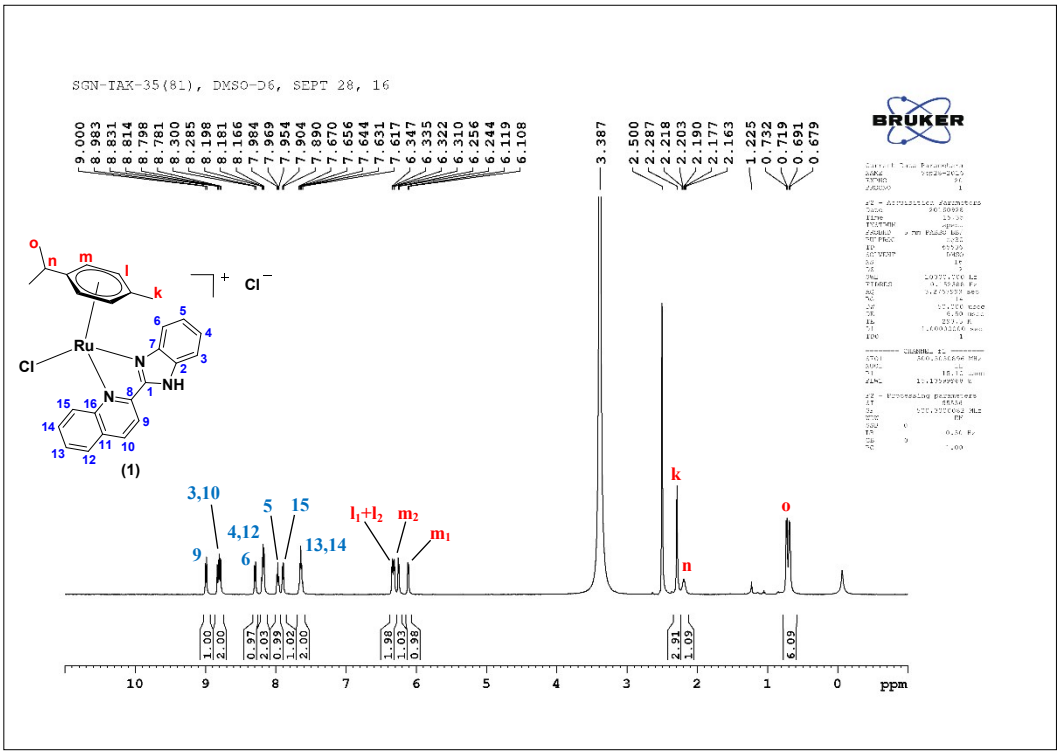

Figure S7. ^{1}H-NMR spectrum of **1** recorded in DMSO-d_6.

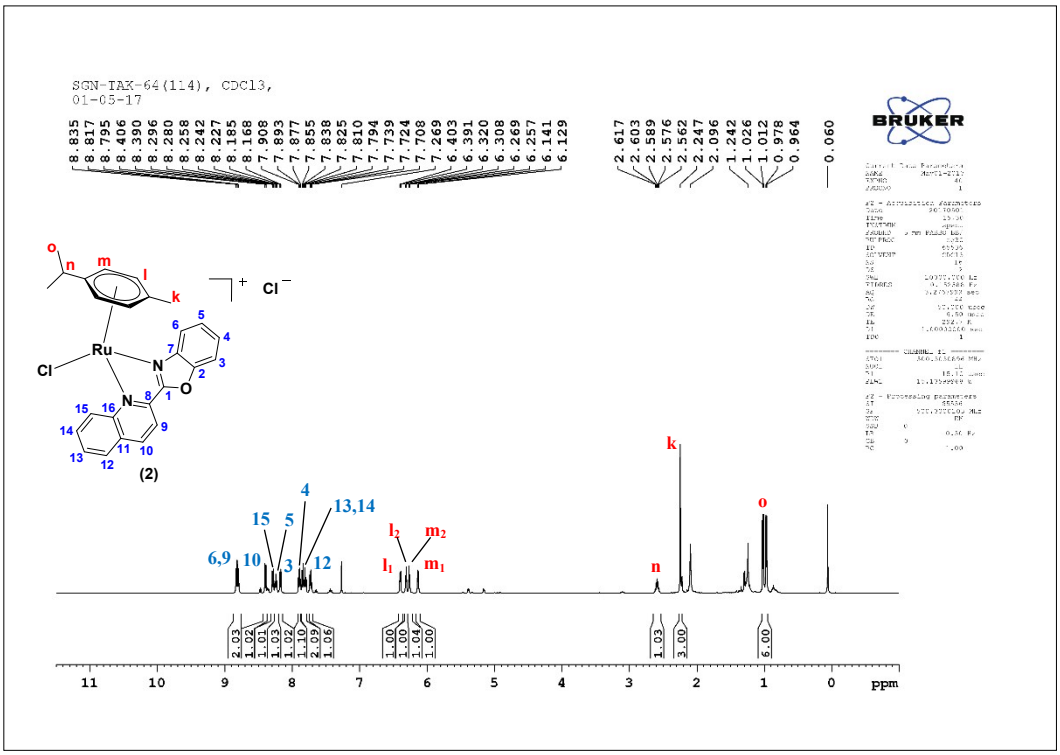

Figure S8. ^{1}H-NMR spectrum of **2** recorded in $CDCl_3$.

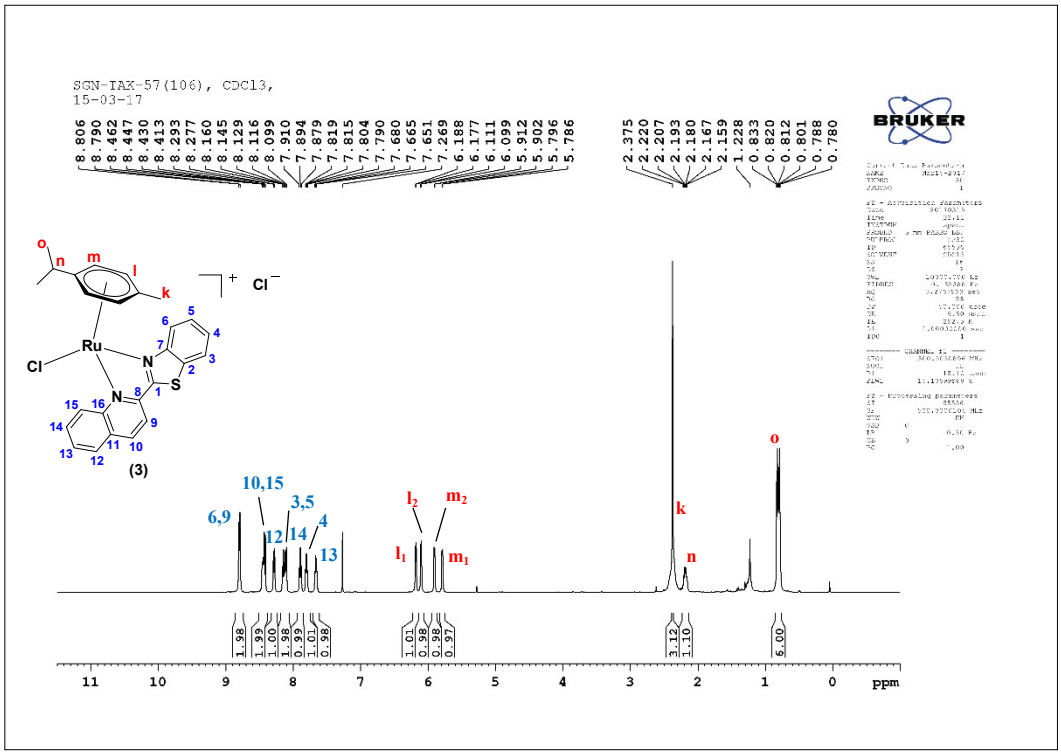

Figure S9. ^{1}H-NMR spectrum of **3** recorded in $CDCl_3$.

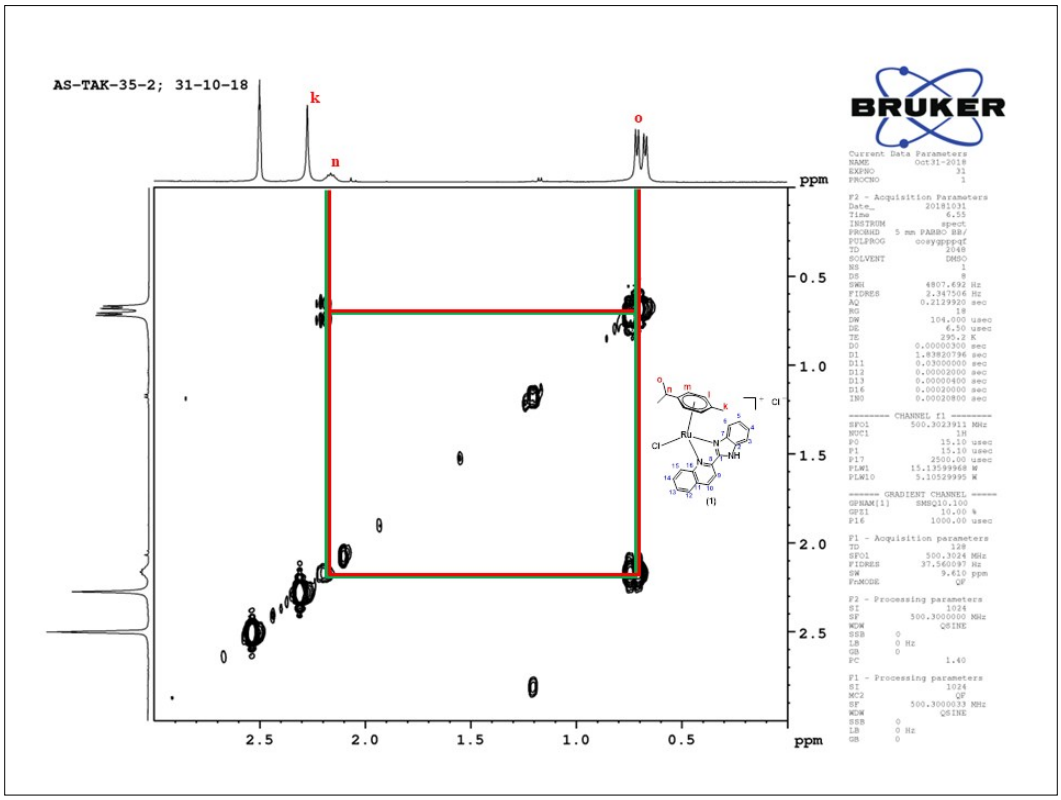

Figure S10. Aliphatic region of ^{1}H-^{1}H-COSY NMR spectrum of **1** recorded in DMSO-d_6.

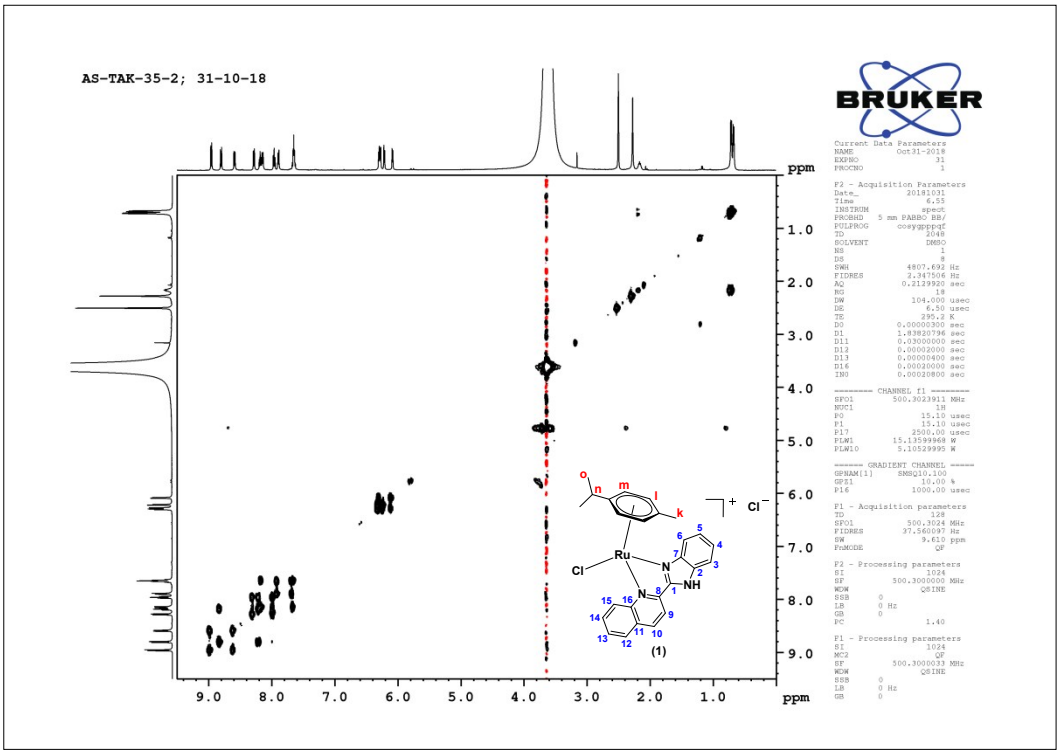

Figure S11. ^{1}H-^{1}H-COSY NMR spectrum of **1** recorded in DMSO-d_6.

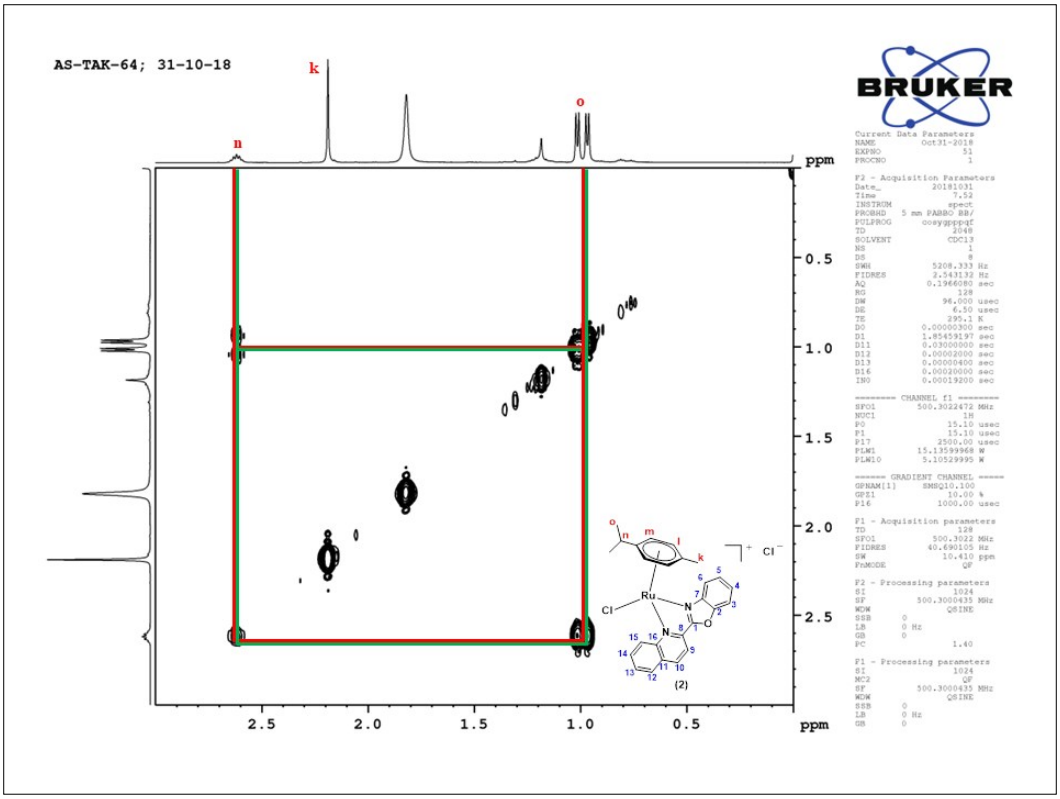

Figure S12. Aliphatic region of ^{1}H-^{1}H-COSY NMR spectrum of **2** recorded in $CDCl_3$.

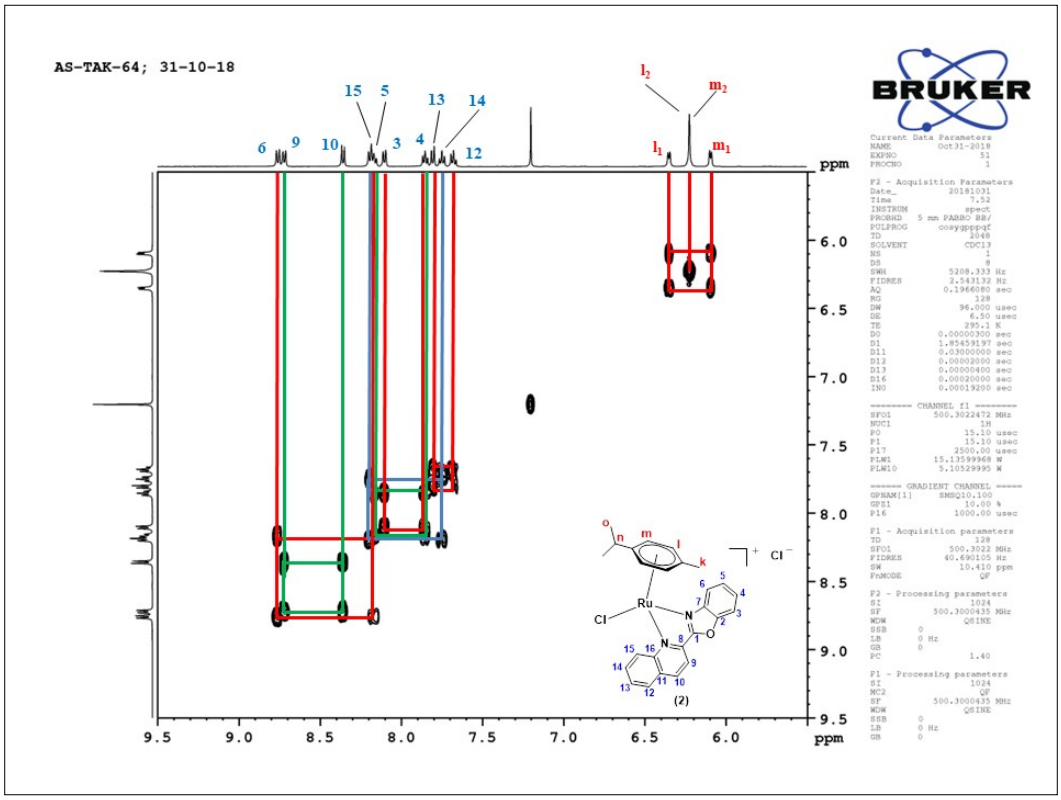

Figure S13. Aromatic region of ^{1}H-^{1}H-COSY NMR spectrum of **2** recorded in $CDCl_3$.

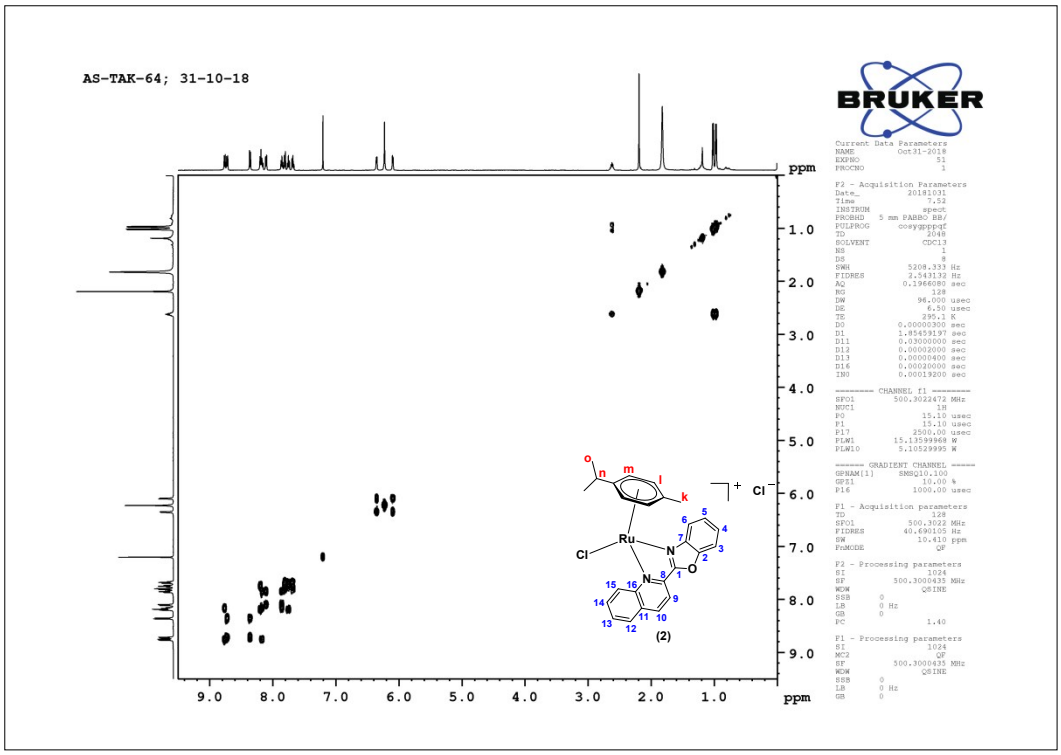

Figure S14. ^{1}H-^{1}H-COSY NMR spectrum of **2** recorded in $CDCl_3$.

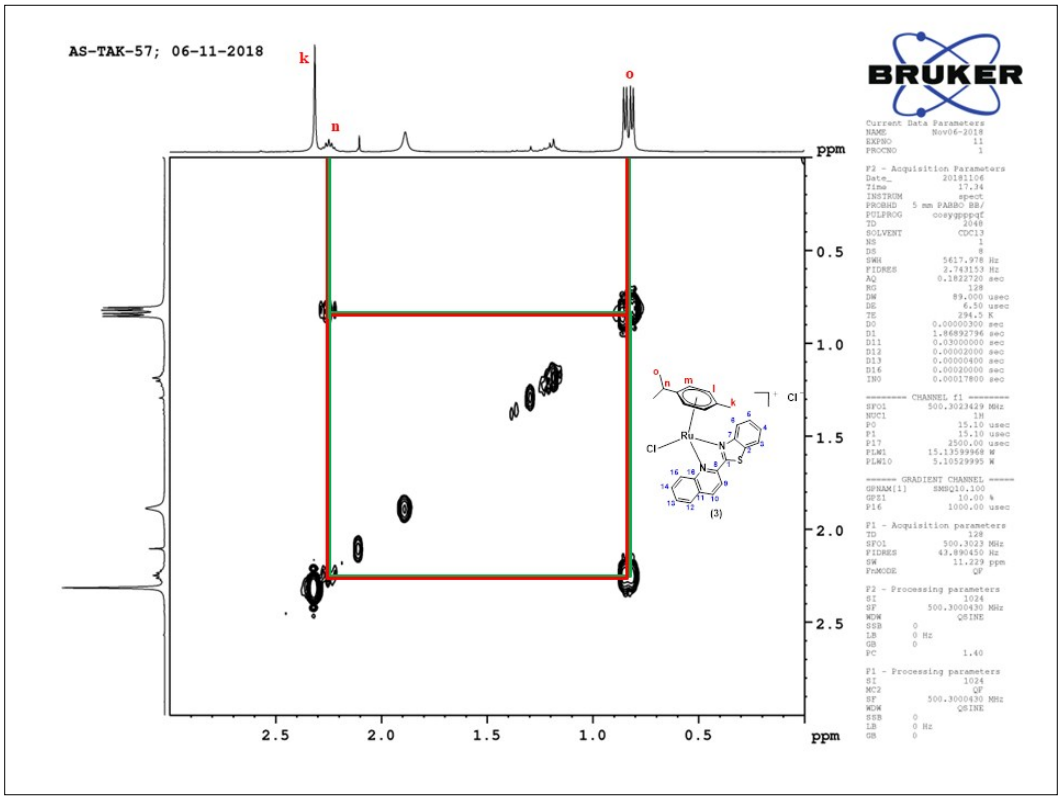

Figure S15. Aliphatic region of ^{1}H-^{1}H-COSY NMR spectrum of **3** recorded in $CDCl_3$.

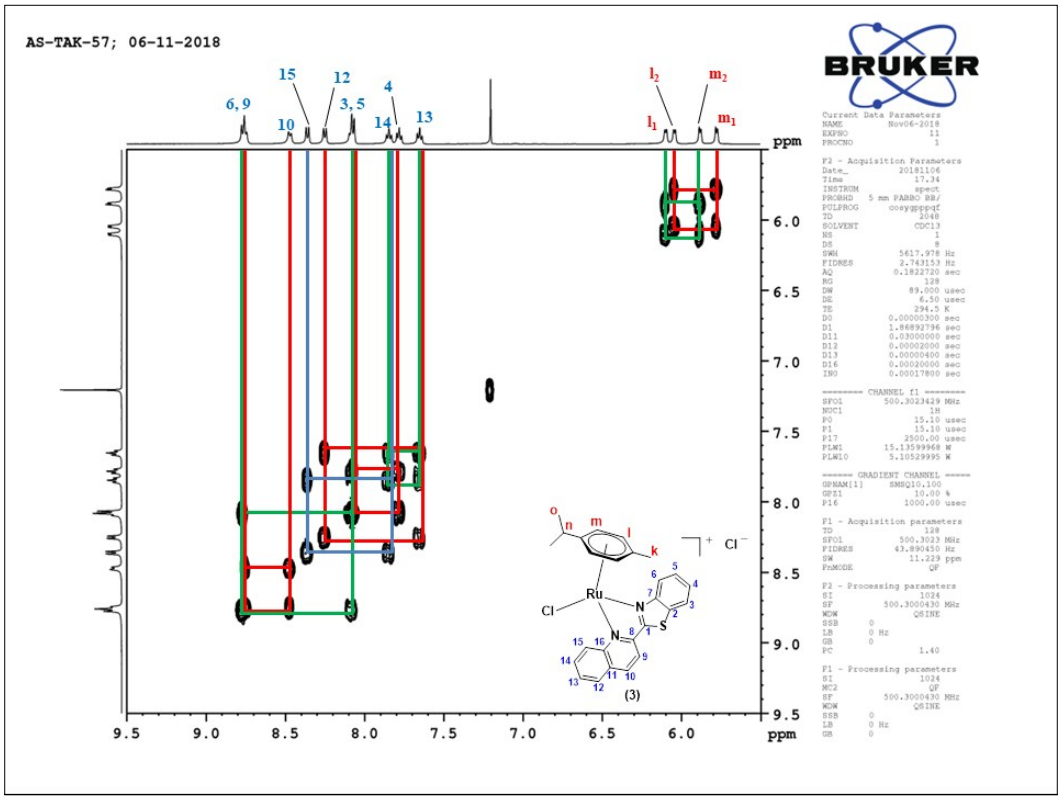

Figure S16. Aromatic region of ^{1}H-^{1}H-COSY NMR spectrum of **3** recorded in $CDCl_3$.

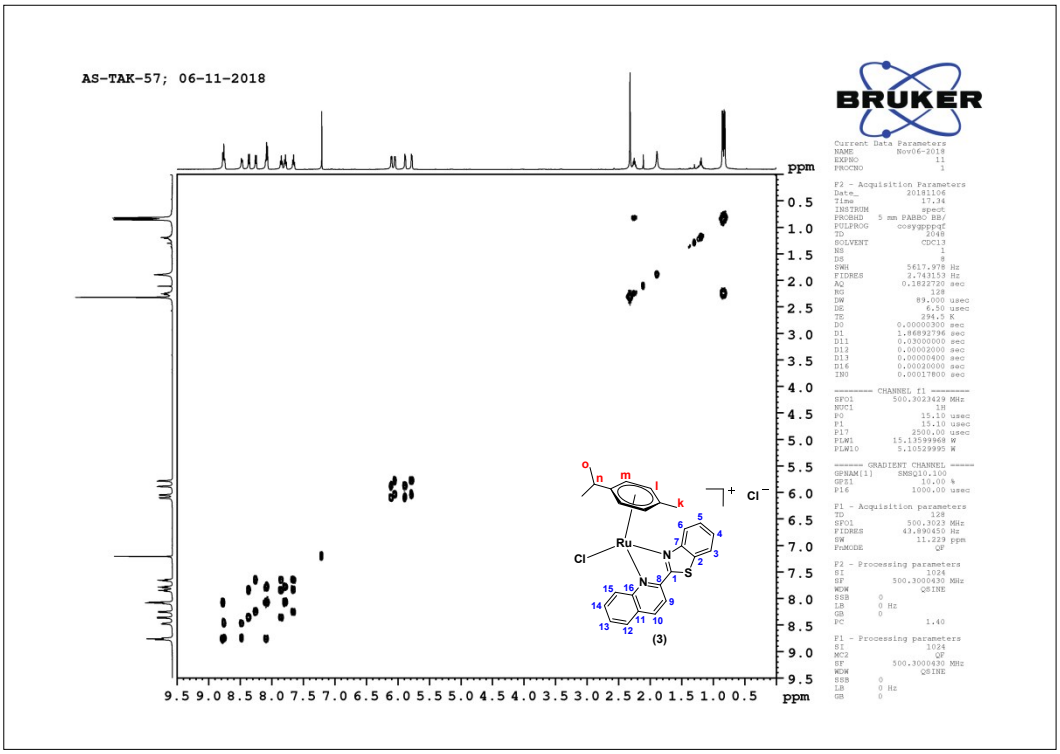

Figure S17. ^{1}H-^{1}H-COSY NMR spectrum of **3** recorded in $CDCl_3$.

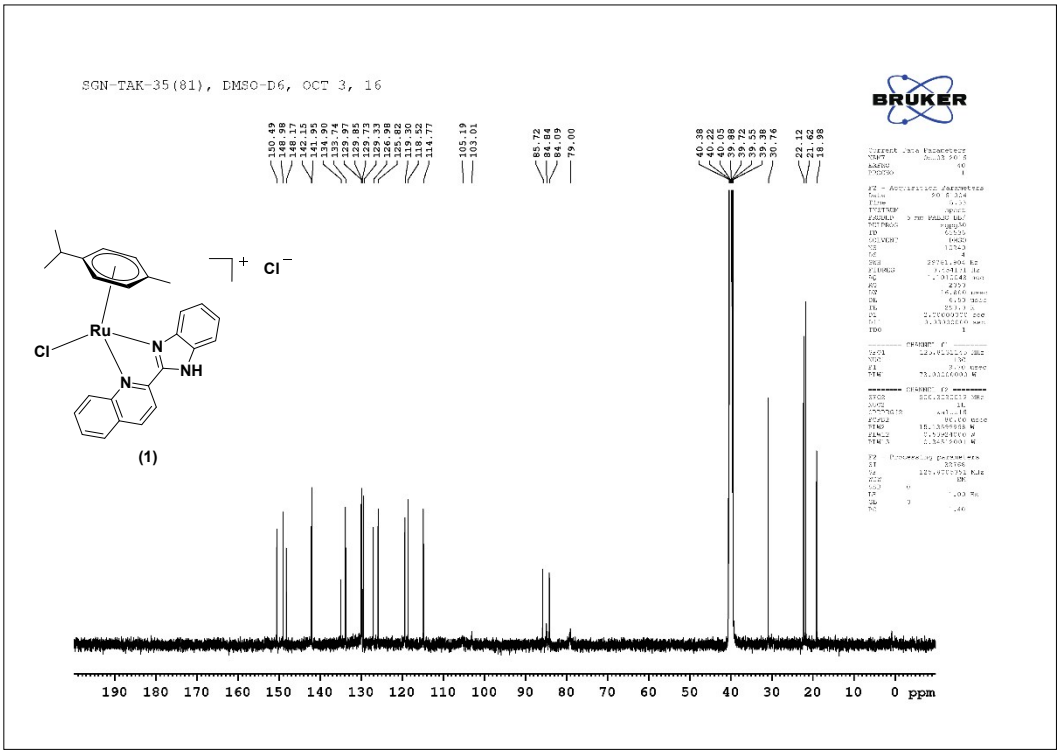

Figure S18. ^{13}C-NMR spectrum of **1** recorded in DMSO-d_6.

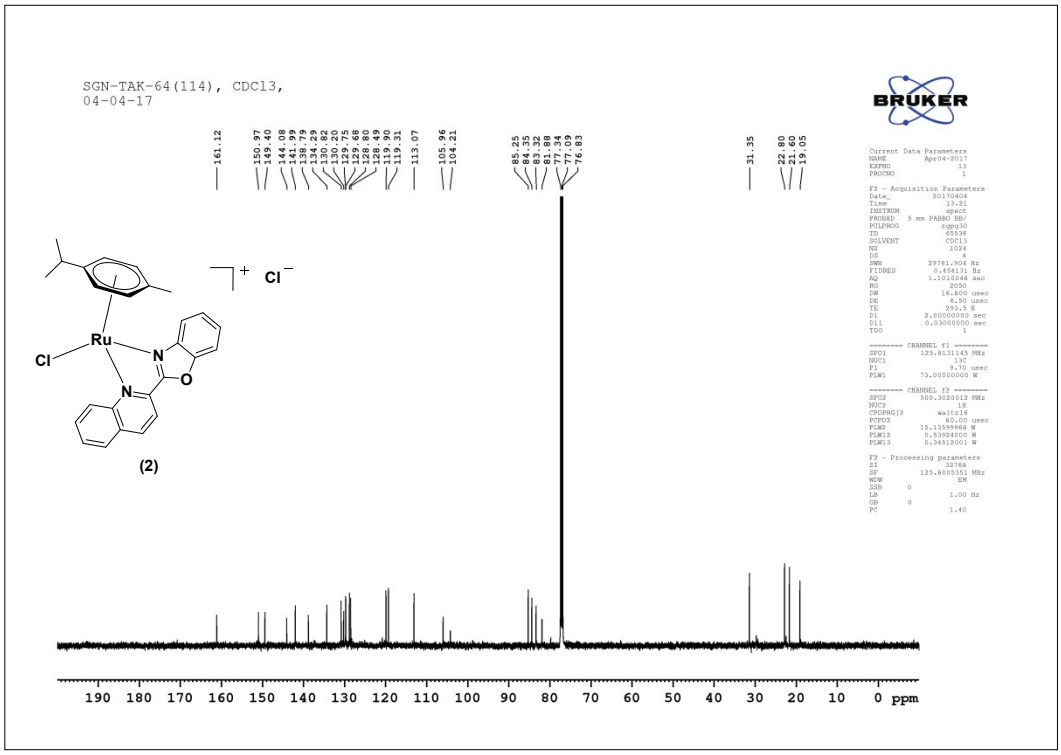

Figure S19. ^{13}C-NMR spectrum of **2** recorded in $CDCl_3$.

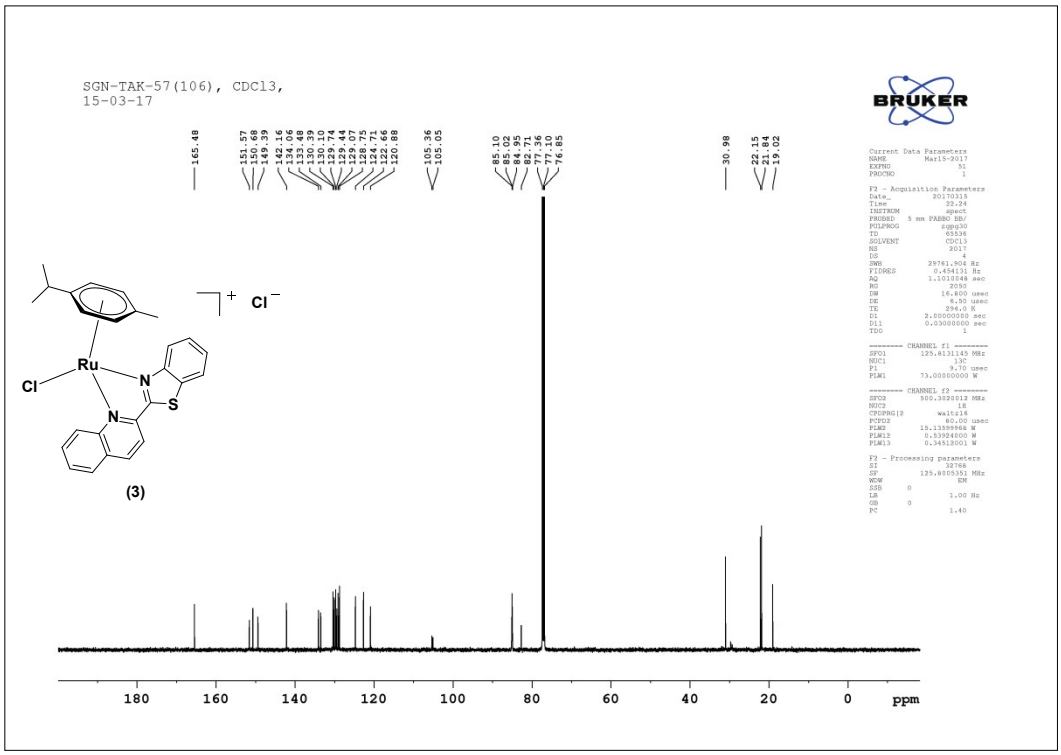

Figure S20. ^{13}C-NMR spectrum of **3** recorded in $CDCl_3$.

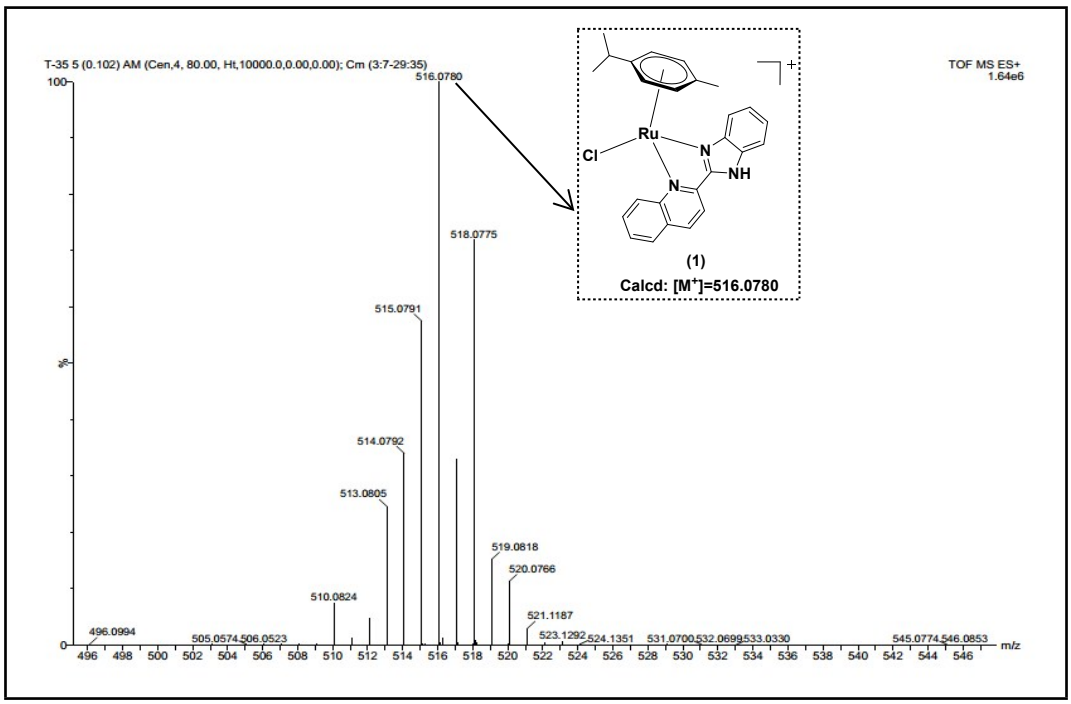

Figure S21. ESI-Mass spectrum of **1** recorded in methanol.

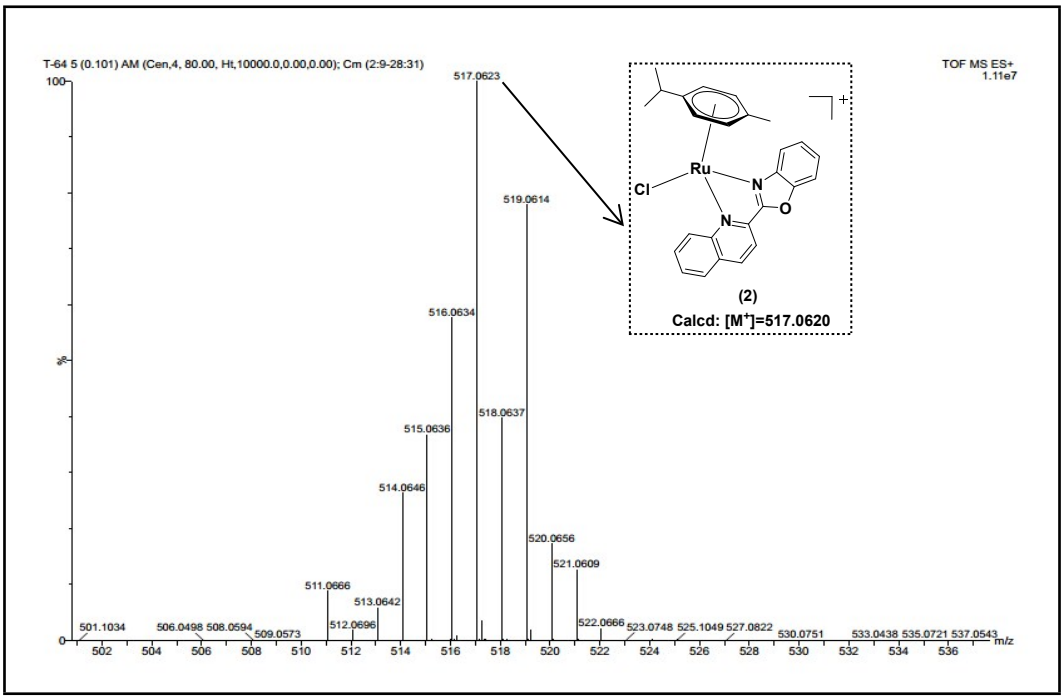

Figure S22. ESI-Mass spectrum of **2** recorded in methanol.

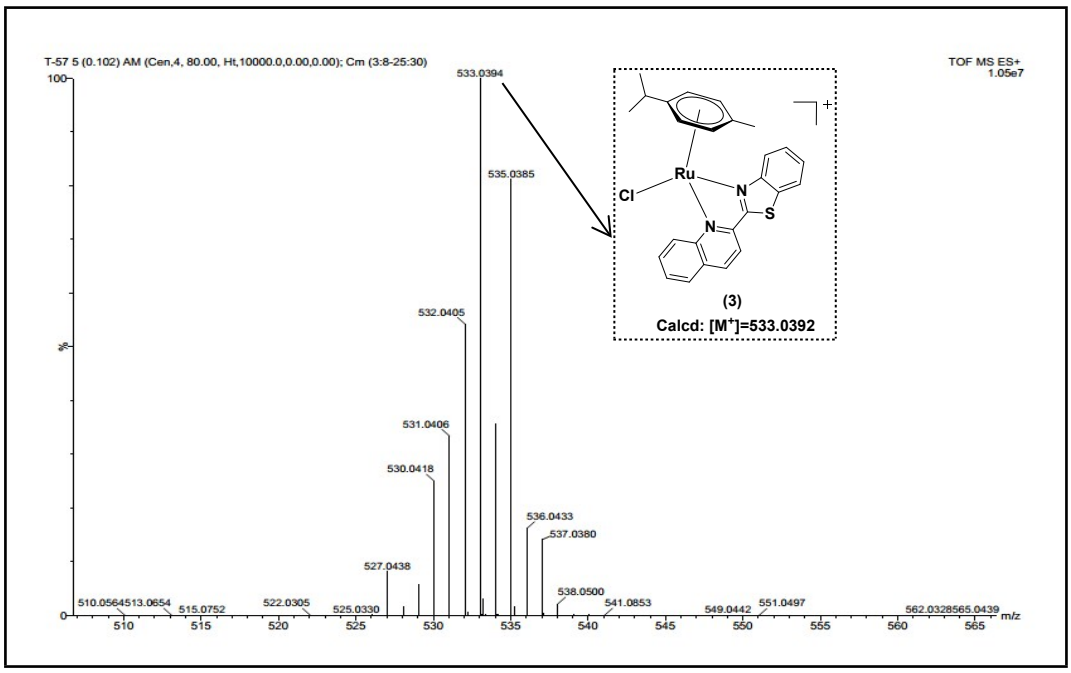

Figure S23. ESI-Mass spectrum of **3** recorded in methanol.

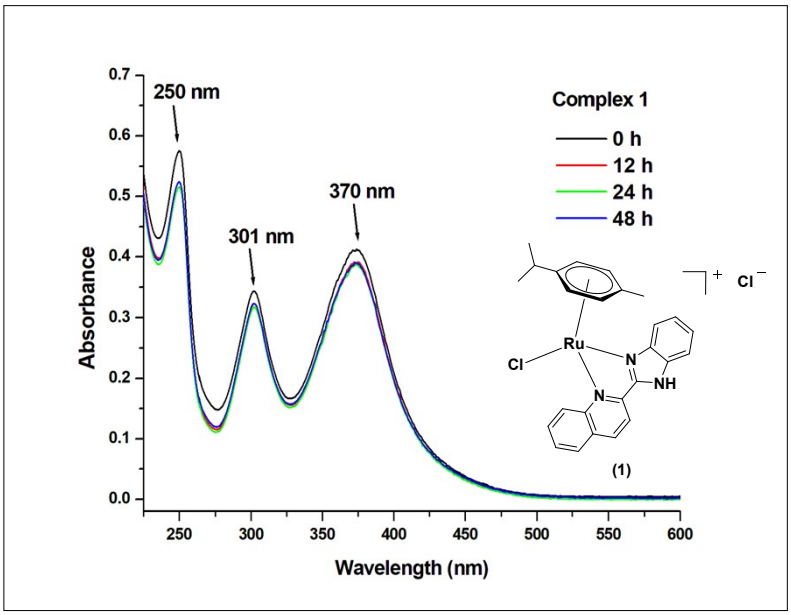

Figure S24. UV- Visible absorption spectra of **1** (26.66 μM) recorded in PBS (pH = 7.4) after 0, 12, 24 and 48 h at 298 K.

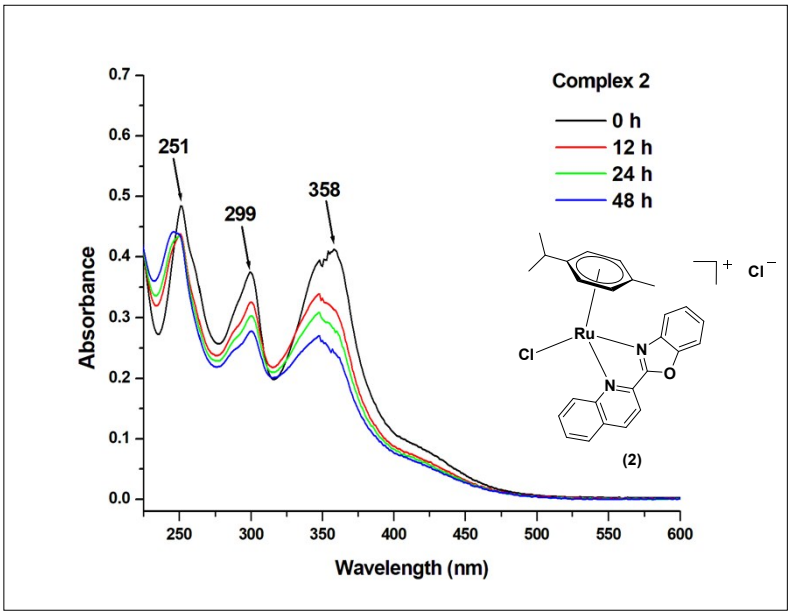

Figure S25A. UV-Visible absorption spectra of **2** (26.66 μM) recorded in PBS (pH = 7.4) after 0, 12, 24 and 48 h at 298 K.

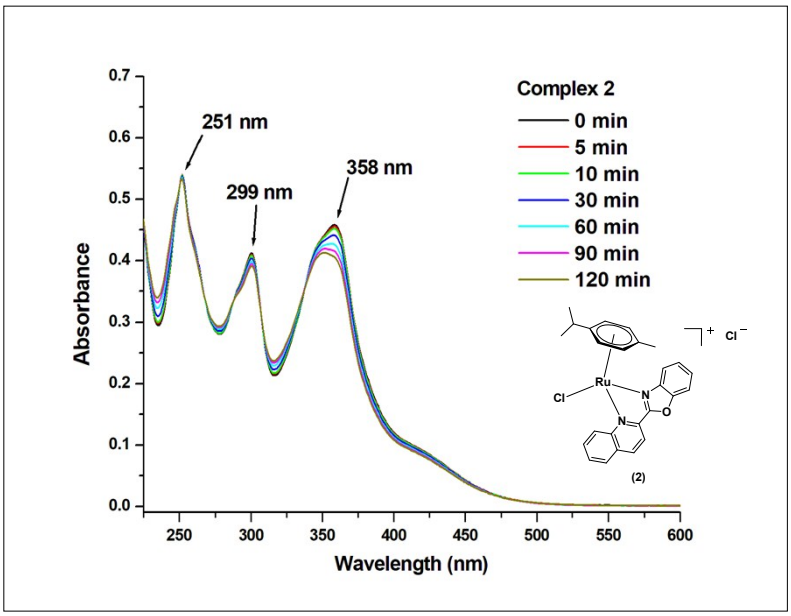

Figure S25B. UV-Visible absorption spectra of **2** (26.66 μM) recorded in PBS (pH = 7.4) after 0, 5, 10, 30, 60, 90 and 120 min at 298 K.

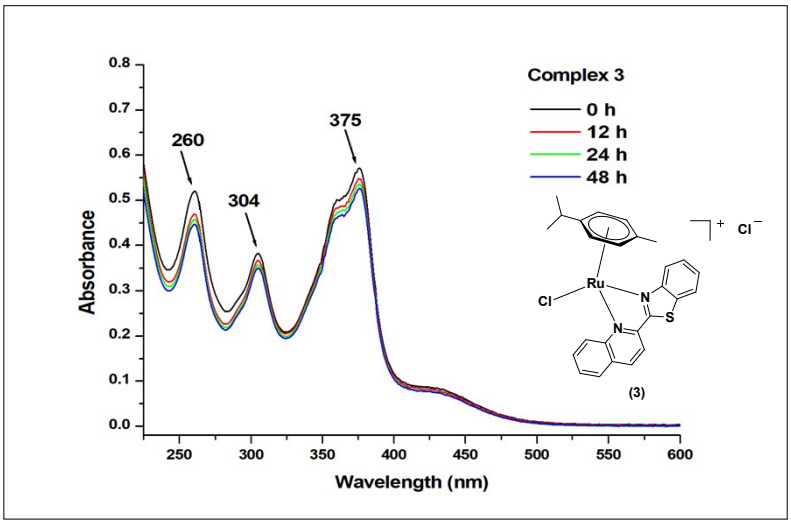

Figure S26. UV-Visible absorption spectra of **3** (26.66 µM) recorded in PBS (pH = 7.4) after 0, 12, 24 and 48 h at 298 K.

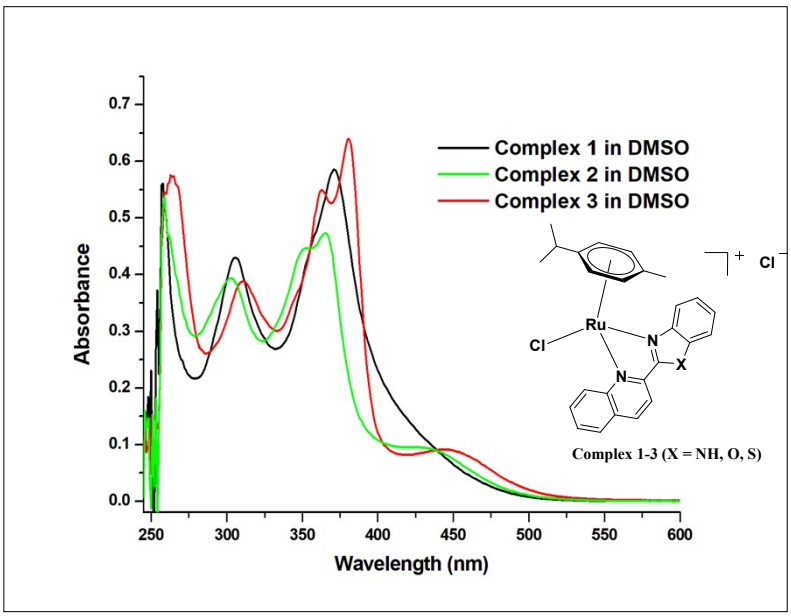

Figure S27. UV-Visible absorption spectra of **1**, **2** and **3** (26.66 µM) recorded in DMSO at 298 K.

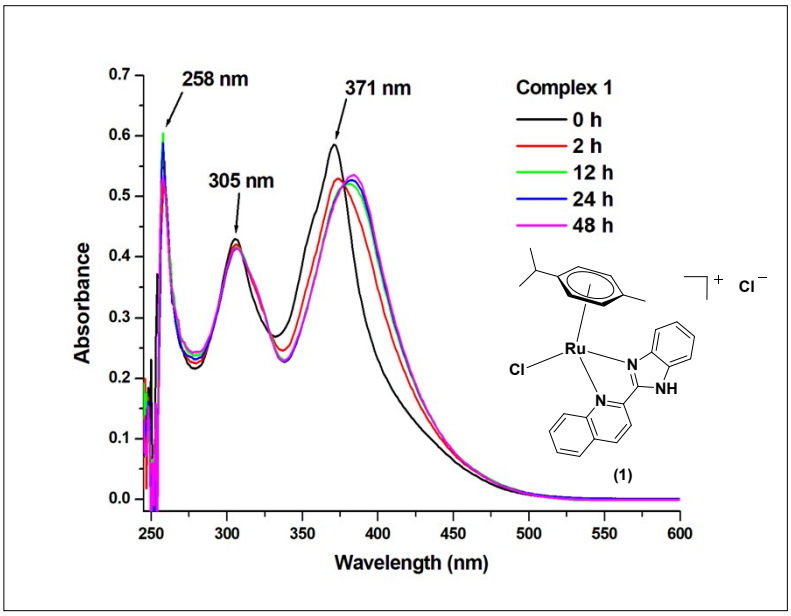

Figure S28. UV-Visible absorption spectra of **1** (26.66 μM) recorded in DMSO after 0, 2, 12, 24 and 48 h at 298 K.

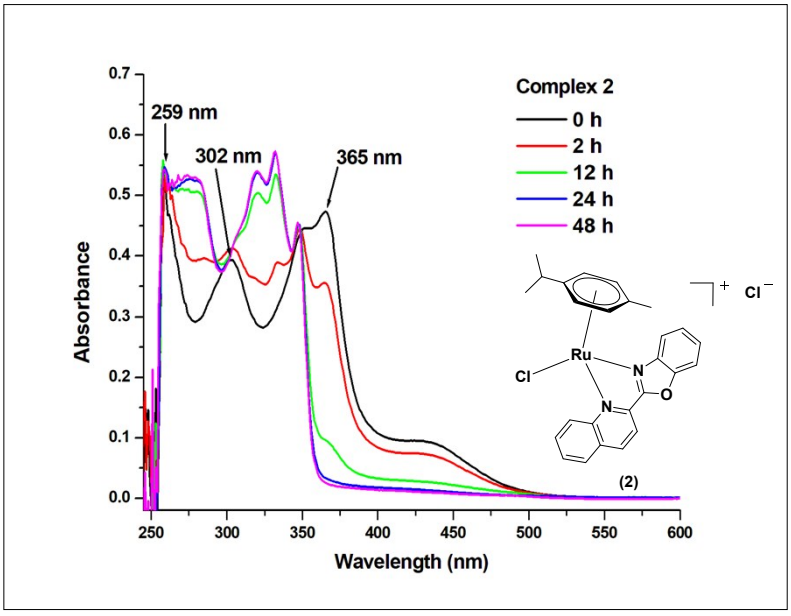

Figure S29. UV-Visible absorption spectra of **2** (26.66 μM) recorded in DMSO after 0, 2, 12, 24 and 48 h at 298 K.

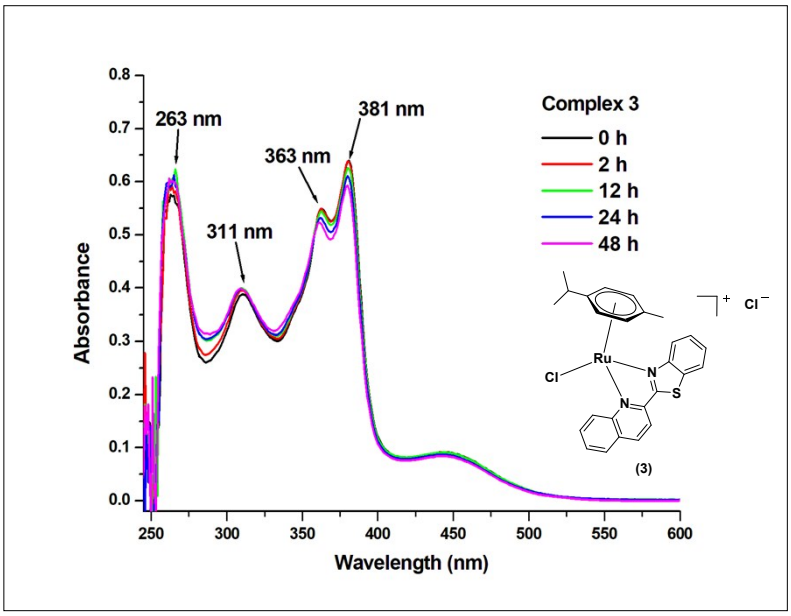

Figure S30. UV-Visible absorption spectra of **3** (26.66 μM) recorded in DMSO after 0, 2, 12, 24 and 48 h at 298 K.

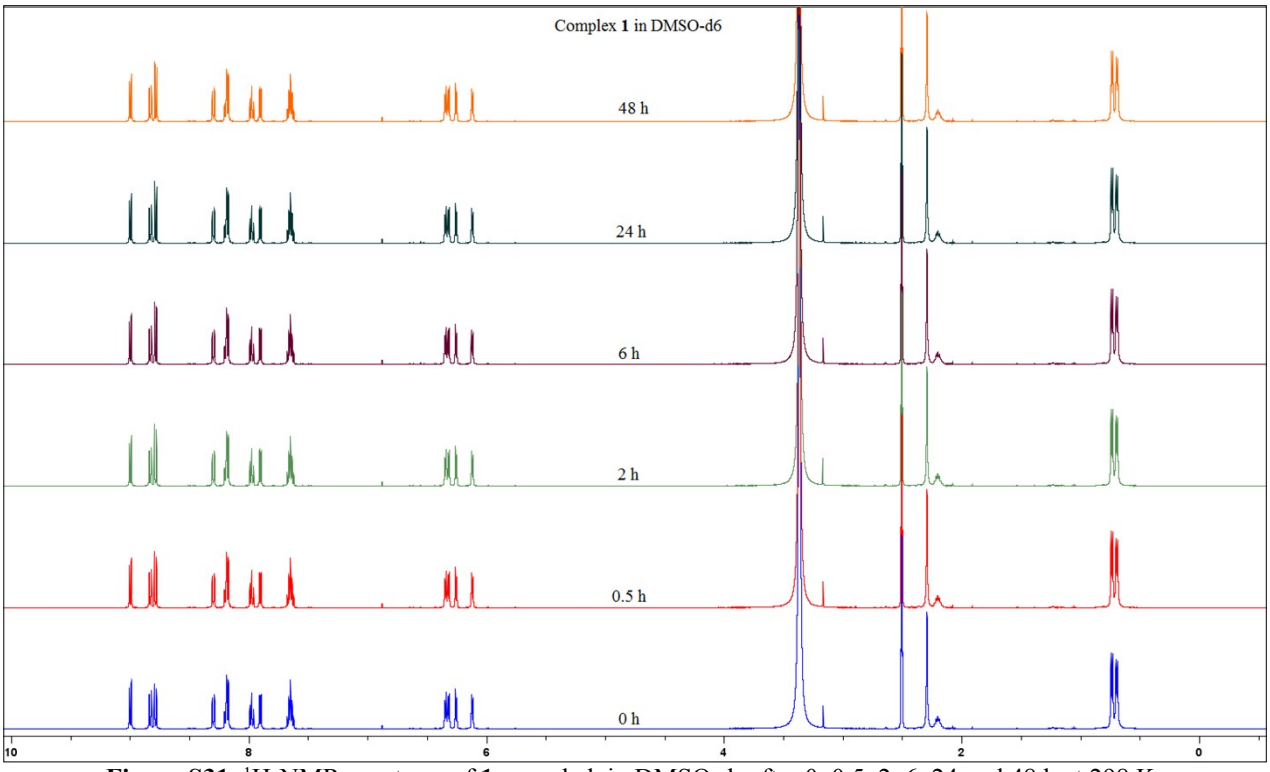

Figure S31. ^{1}H-NMR spectrum of **1** recorded in DMSO-d_6 after 0, 0.5, 2, 6, 24 and 48 h at 298 K.

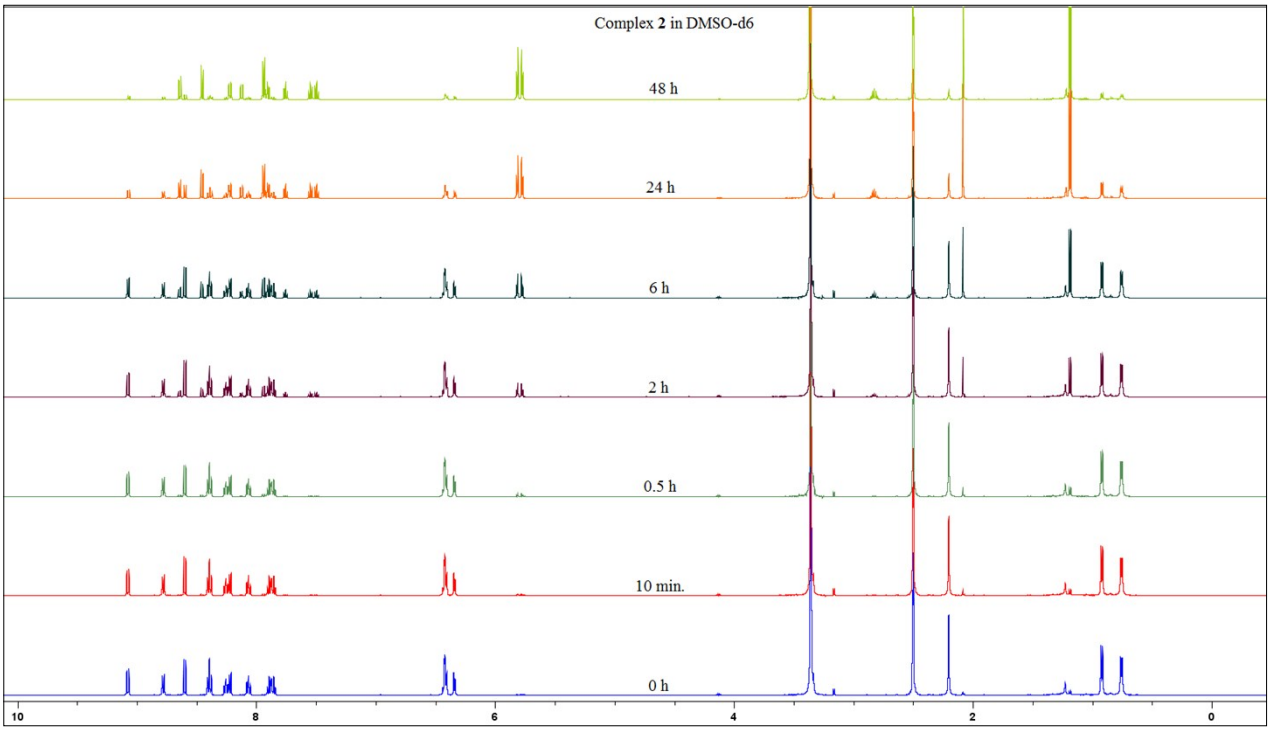

Figure S32. ^{1}H-NMR spectrum of **2** recorded in DMSO-d_6 after 0 h, 10 min., 0.5 h, 2 h, 6 h, 24 h and 48 h at 298 K.

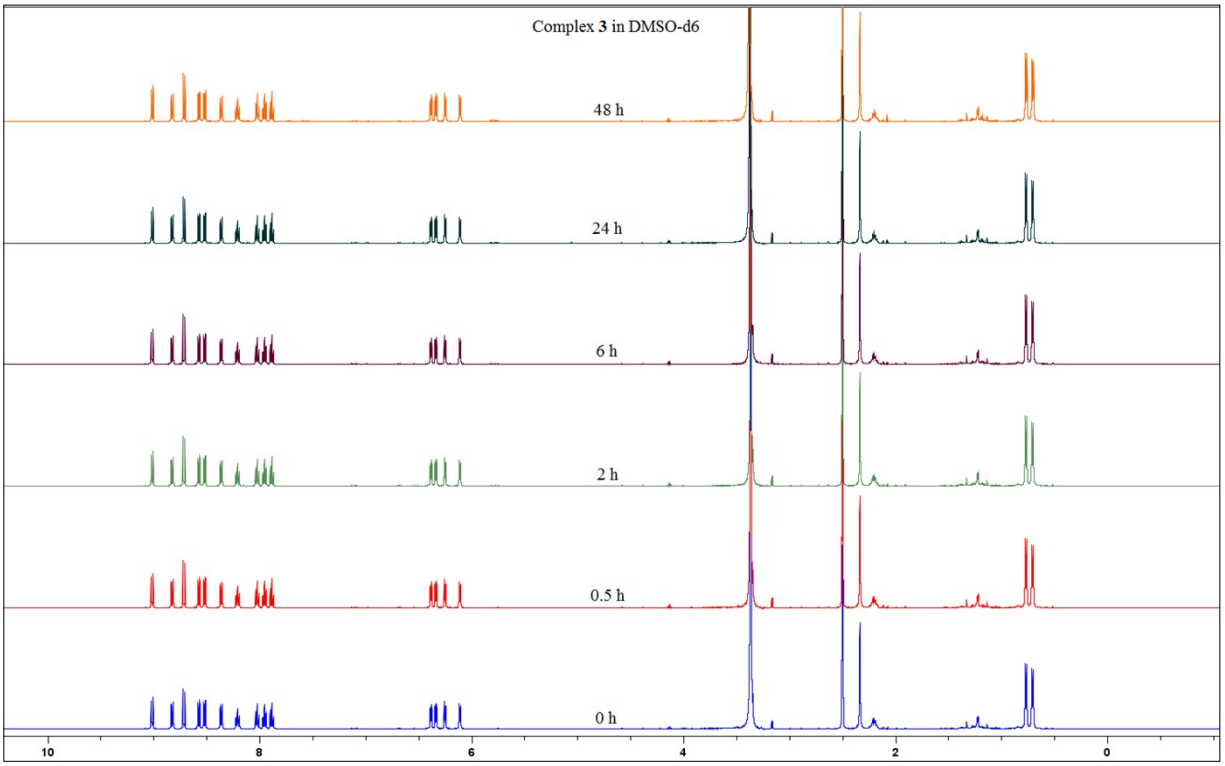

Figure S33. ^{1}H-NMR spectrum of **3** recorded in DMSO-d_6 after 0, 0.5, 2, 6, 24 and 48 h at 298 K.

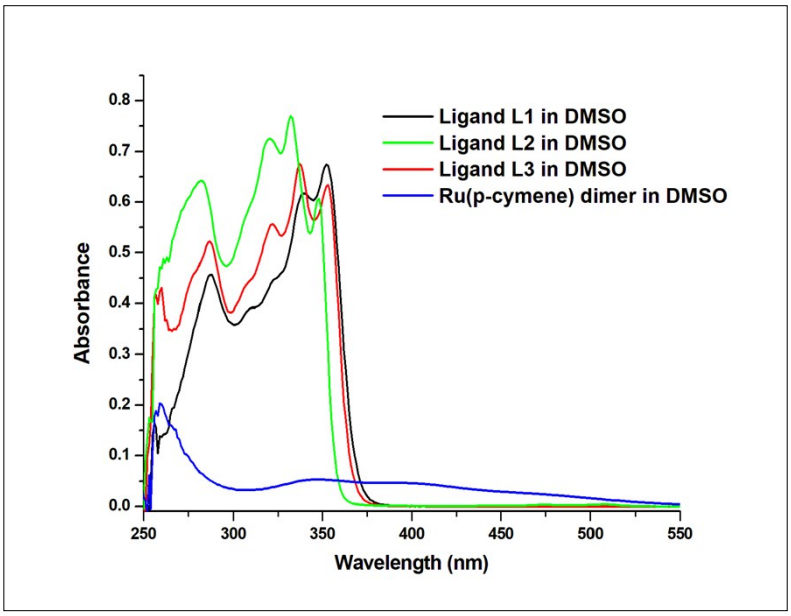

Figure S34. UV-Visible absorption spectra of $\mathbf{L_1}$, $\mathbf{L_2}$, $\mathbf{L_3}$and Ru(p-cymene)dimer (26.66 µM) recorded in DMSO at 298 K.

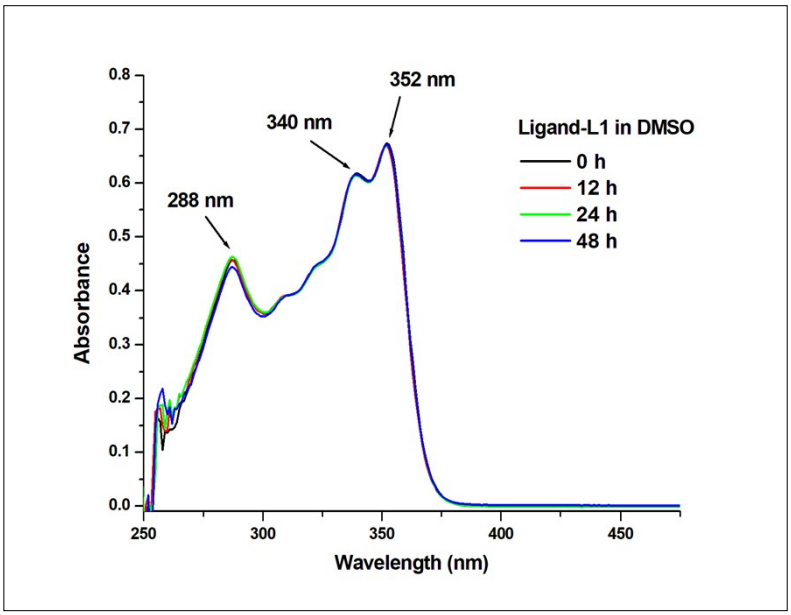

Figure S35. UV-Visible absorption spectra of $\mathbf{L_1}$ (26.66 µM) recorded in DMSO after 0, 12, 24 and 48 h at 298 K.

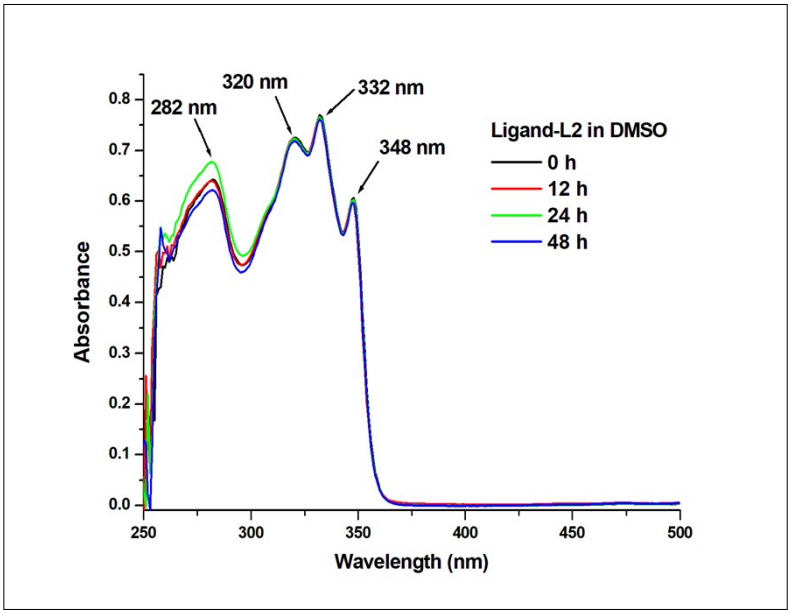

Figure S36. UV-Visible absorption spectra of $\mathbf{L_2}$ (26.66 μM) recorded in DMSO after 0, 12, 24 and 48 h at 298 K.

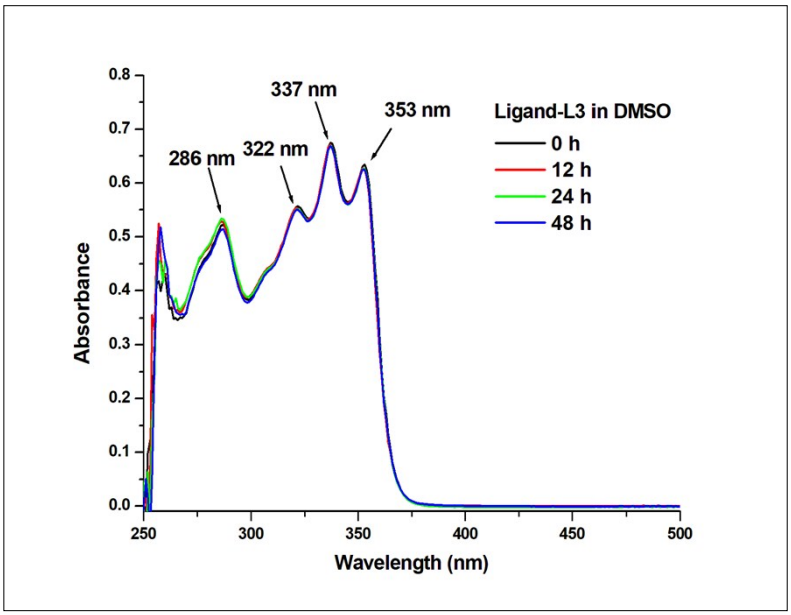

Figure S37. UV-Visible absorption spectra of $\mathbf{L_3}$ (26.66 μM) recorded in DMSO after 0, 12, 24 and 48 h at 298 K.

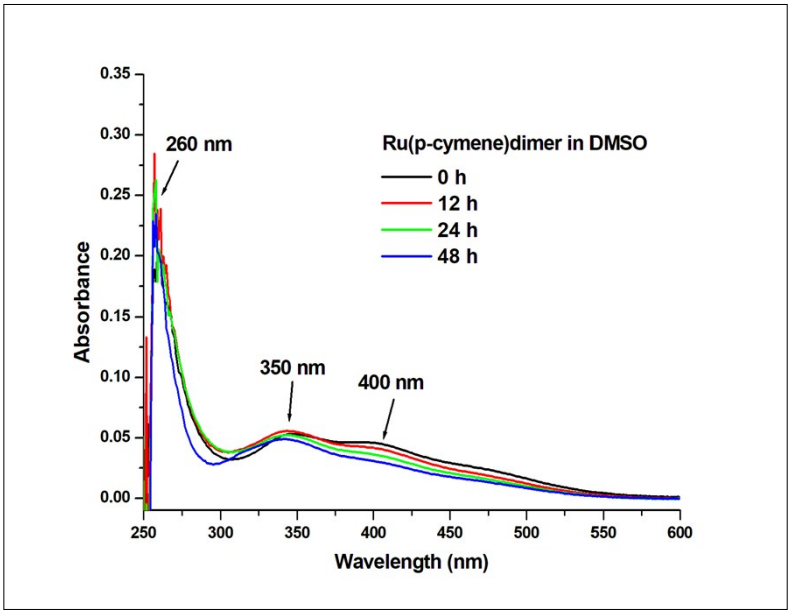

Figure S38. UV-Visible absorption spectra of Ru(p-cymene)dimer (26.66 μM) recorded in DMSO after 0, 12, 24 and 48 h at 298 K.

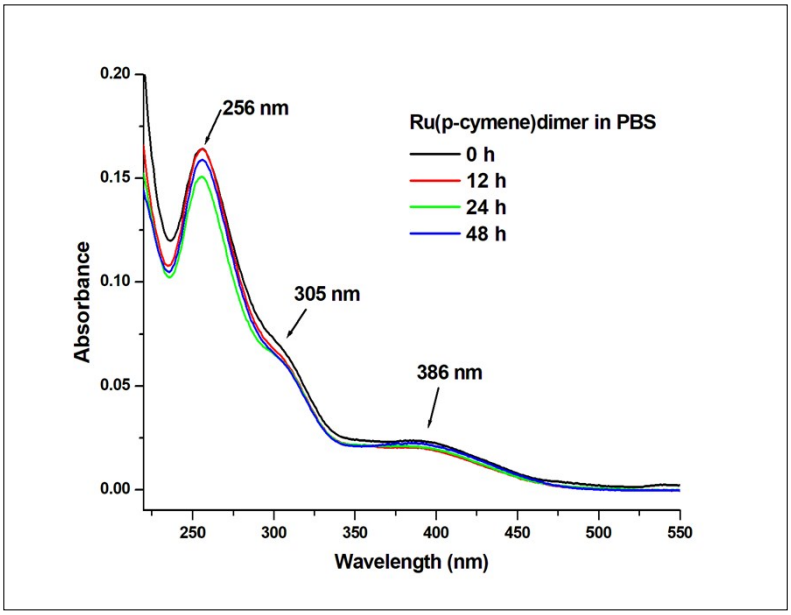

Figure S39. UV-Visible absorption spectra of Ru(p-cymene)dimer (26.66 μM) recorded in PBS (pH = 7.4) after 0, 12, 24 and 48 h at 298 K.

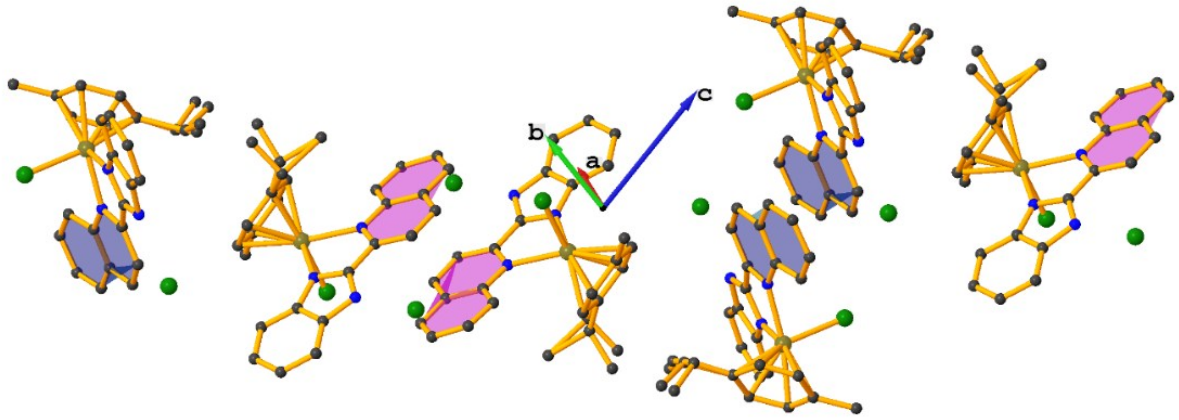

Figure S40. Demonstrating intermolecular π-π stacking interactions for **1**; [Hydrogen atoms and solvent molecules omitted for clarity].

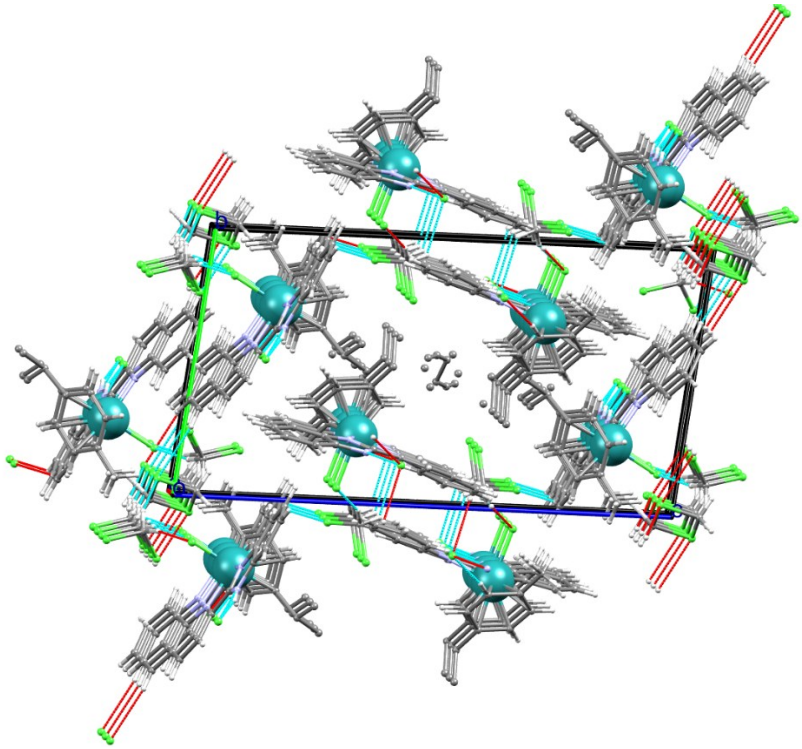

Figure S41. Showing C-H···Cl and N-H···Cl hydrogen bonded network in crystal structure of **1**.

Table S1. Selected bond distances and bond angles (Å, º) observed in crystal structure of **1**.

Molecule 1	**Bond Distance**	**Molecule 2**	**Bond Distance**
Ru1-N1	2.171(5)	Ru2-N4	2.170(5)
Ru1-N2	2.072(5)	Ru2-N5	2.075(5)
Ru1-C1	2.250(7)	Ru2-C27	2.235(7)
Ru1-C2	2.191(6)	Ru2-C28	2.198(7)
Ru1-C3	2.167(7)	Ru2-C29	2.175(7)
Ru1-C4	2.182(8)	Ru2-C30	2.201(9)
Ru1-C5	2.169(8)	Ru2-C31	2.170(8)

Ru1-C6	2.223(8)	Ru2-C32	2.227(7)
Ru1-Cl1	2.3901(16)	Ru2-Cl2	2.3966(18)
Molecule 1	**Bond Angle**	**Molecule 2**	**Bond Angle**
N2-Ru1-N1	75.88(19)	N5-Ru2-N4	76.07(19)
N1-Ru1-Cl1	85.33(13)	N4-Ru2-Cl2	86.20(13)
N2-Ru1-Cl1	86.87(15)	N5-Ru2-Cl2	86.36(14)

Table S2. π···π interaction parameters (Å, º) associated with crystal structure of **1**.

Cg···Cg	Cg···Cg	Dihedral angle	Slippage	Symmetry
Cg(2)···Cg(2)	3.690(4)	0.0(3)	1.409	2-x,2-y,1-z
Cg(2)···Cg(4)	3.779(4)	4.5(3)	1.816	2-x,2-y,1-z
Cg(7)···Cg(7)	3.762(4)	0.0(3)	1.746	1-x,1-y,2-z
Cg(7)···Cg(9)	3.632(4)	5.4(3)	1.686	1-x,1-y,2-z

Cg(2): N4-C37-C38-C39-C40-C45; Cg(4): C40-C41-C42-C43-C44-C45; Cg(7): N1-C11-C12-C13-C14-C19; Cg(9): C14-C15-C16-C17-C18-C19

Table S3. Hydrogen bond parameters (Å, º) associated with crystal structure of **1**.

X-H···Y	**X-H**	**H···Y**	**X···Y**	**X-H···Y**	**Symmetry**
N3-H3S···Cl3	0.78(10)	2.21(10)	2.967(6)	165(8)	
C15-H15···Cl9	0.9300	2.8300	3.555(7)	136.00	1-x,1-y,2-z
C24-H24···Cl7	0.9300	2.7600	3.523(9)	140.00	x,-1+y,z
C32-H32···Cl4	0.9300	2.6500	3.575(11)	173.00	-1+x,y,z
C33-H33C···Cl2	0.9600	2.7800	3.353(11)	119.00	
C53-H53A···Cl2	0.9700	2.6900	3.619(9)	160.00	1+x,y,z
C53-H53B···Cl4	0.9700	2.8000	3.531(9)	133.00	
C54-H54A···Cl1	0.9700	2.7200	3.668(10)	166.00	1-x,1-y,2-z

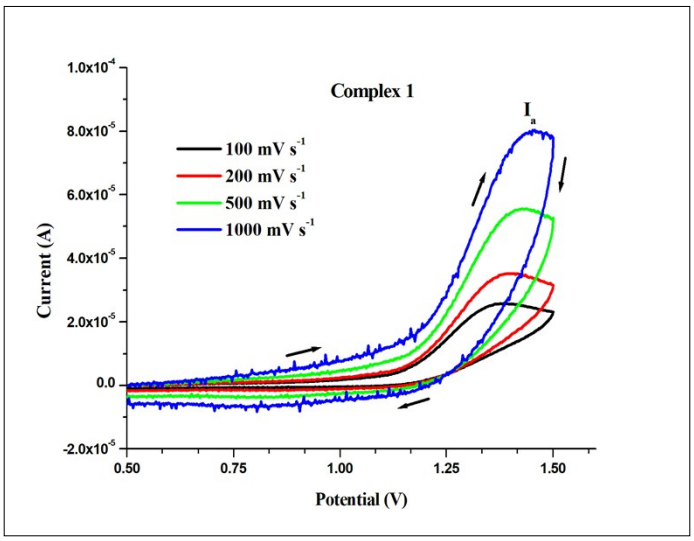

Figure S42. Cyclic voltammograms of 1 (1 mM) solution in CH_3CN with 0.1 M [nBu_4N][ClO_4] at scan rates: 100 mV s^{-1}, 200 mV s^{-1}, 500 mV s^{-1}, 1000 mV s^{-1} at room temperature (Range: 0.5 to 1.5 V).

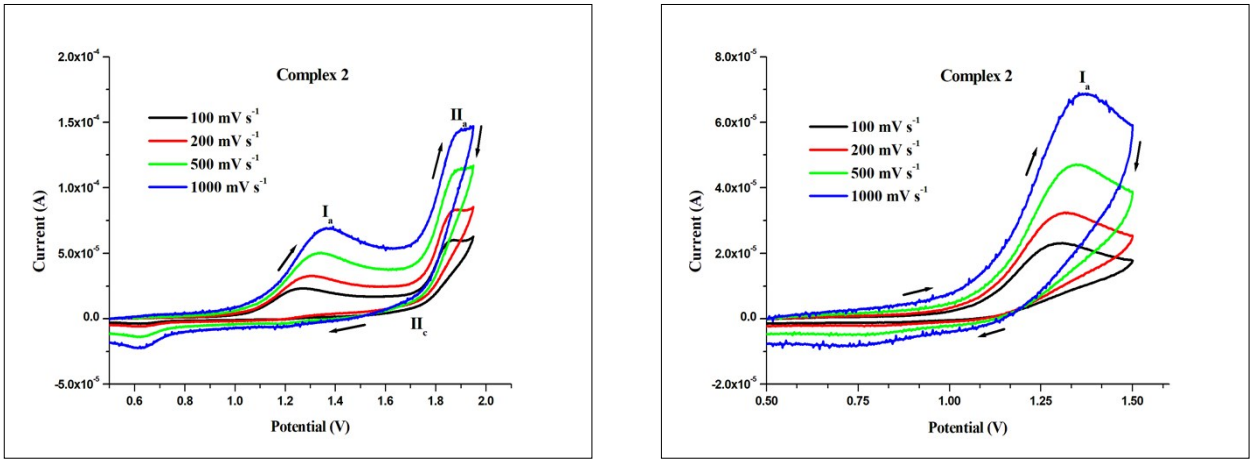

Figure S43. Cyclic voltammograms of **2** (1 mM) solution in CH_3CN with 0.1 M $[nBu_4N][ClO_4]$ at scan rates: 100 mV s^{-1}, 200 mV s^{-1}, 500 mV s^{-1}, 1000 mV s^{-1} at room temperature (Range: 0.5 to 1.95 V and 0.5 to 1.5 V).

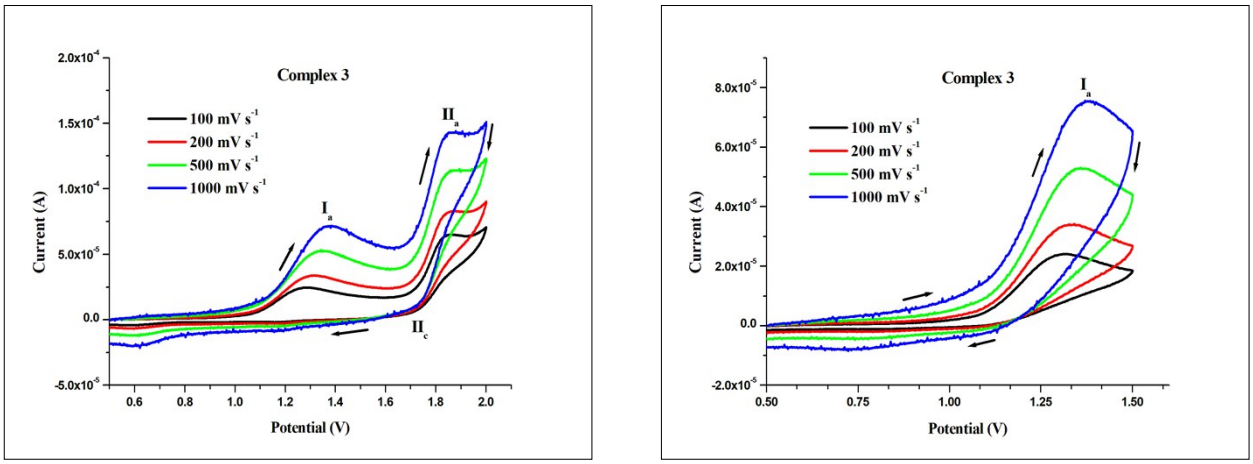

Figure S44. Cyclic voltammograms of **3** (1 mM) solution in CH_3CN with 0.1 M $[nBu_4N][ClO_4]$ at scan rates: 100 mV s^{-1}, 200 mV s^{-1}, 500 mV s^{-1}, 1000 mV s^{-1} at room temperature (Range: 0.5 to 2.0 V and 0.5 to 1.5 V).

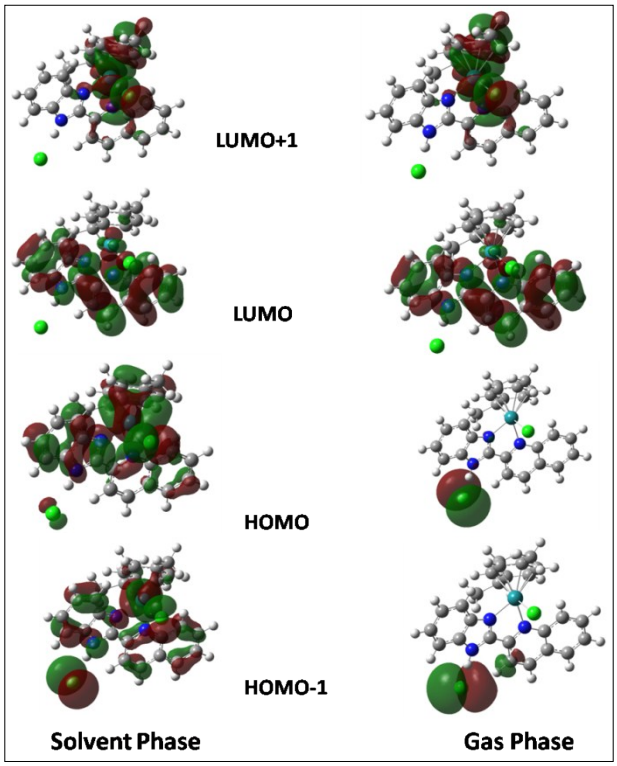

Figure S45A. DFT optimized structures of the global minima (with and without solvent) with frontier MOs of **1**.

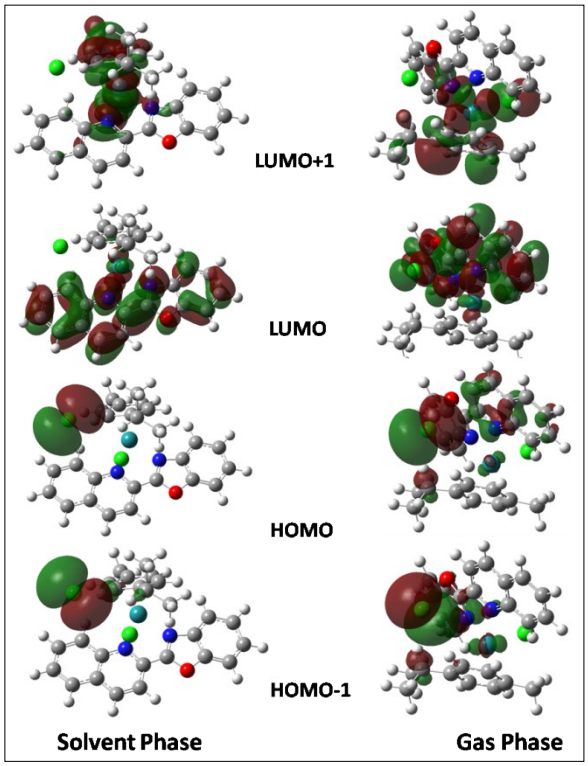

Figure S45B. DFT optimized structures of the global minima (with and without solvent) with frontier MOs of **2**.

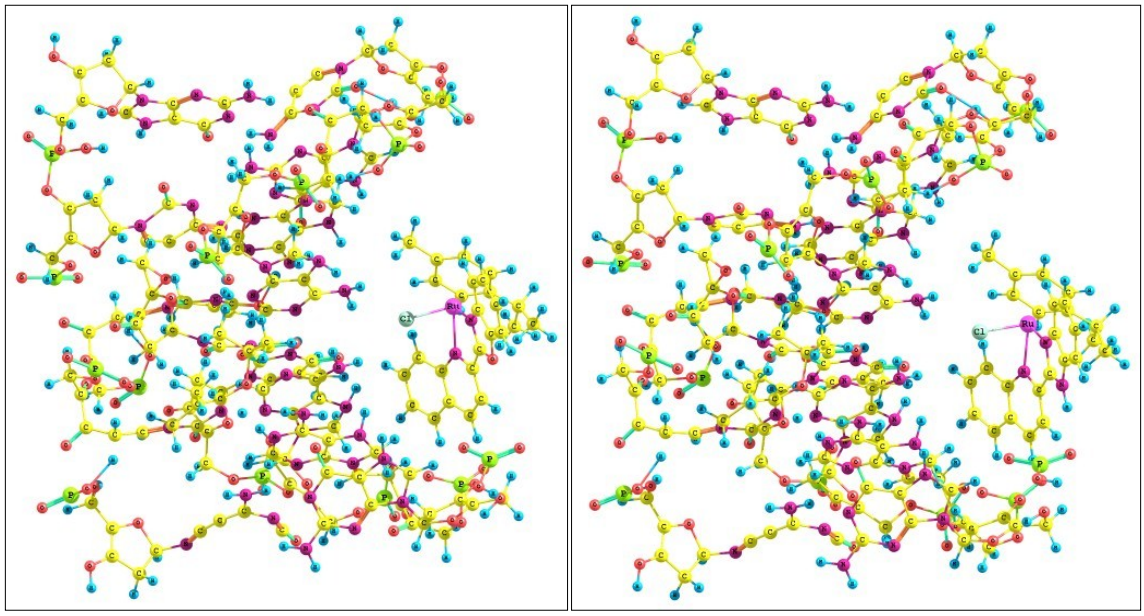

Figure S46. Molecular docked model of **1** (right column) and **2** (left column) with B-DNA optimized at PM6 method.

Table S4. Selected bond lengths (Å) and bond angles (˚) of **1** in DFT optimized structures (at B3LYP/6-31G(d,p)/LanL2DZ level of theory)with and without solvent.

Structure: 1	**Bond length (Å)**		
	Gas phase	**Solvent phase**	**Reference[1]**
N1–Ru	2.082	2.090	2.122
N2–Ru	2.159	2.169	2.147
Ru-Cl	2.418	2.453	-
Ru- C (ή^6 Phe)	2.250 2.310 2.261 2.293 2.337 2.291	2.338 2.292 2.253 2.308 2.276 2.301	2.261 2.278 2.259 2.286 2.268 2.288
N3-H	1.107	1.052	-
H...Cl$^-$	1.812	2.020	-
	Bond Angles (˚)		
N1–Ru-N2	76.71	76.57	80.41
N1–Ru-Cl	87.82	87.27	84.58
N2–Ru-Cl	85.91	85.97	82.28

Table S5. Selected bond lengths (Å) and bond angles (˚) of **2** in DFT optimized structures (at B3LYP/6-31G(d,p)/LanL2DZ level of theory) of with and without solvent for four different conformers **A, B, C** and **D**.

Structure: 2	**Bond length (Å)**								
	A		**B**		**C**		**D**		**Reference[1]**
	Gas phase	**Solvent phase**	**Gas phase**	**Solvent phase**	**Gas phase**	**Solvent phase**	**Gas phase**	**Solvent phase**	
N1–Ru	2.098	2.103	2.112	2.106	2.131	2.106	2.107	2.107	2.122

N2–Ru	2.178	2.198	2.213	2.185	2.238	2.186	2.223	2.194	2.147
Ru-Cl	2.431	2.452	2.428	2.452	2.467	2.456	2.429	2.453	-
Ru- C (ή⁶ Phe)	2.276 2.374 2.292 2.264 2.308 2.237	2.246 2.327 2.292 2.303 2.333 2.271	2.291 2.332 2.251 2.282 2.326 2.287	2.256 2.308 2.276 2.287 2.336 2.300	2.661 2.295 2.196 2.236 2.252 2.225	2.278 2.319 2.278 2.282 2.323 2.287	2.287 2.347 2.264 2.310 2.347 2.262	2.273 2.320 2.266 2.286 2.329 2.285	2.261 2.278 2.259 2.286 2.268 2.288
H...Cl⁻	2.445	2.49939	2.353	2.466	2.406	2.460	2.132	2.458	-
	Bond Angles (˚)								
N1–Ru-N2	75.91	76.52	76.70	76.64	75.49	76.58	76.74	76.51	80.41
N1–Ru-Cl	87.80	86.51	85.28	87.04	84.88	86.56	84.79	86.21	84.58
N2–Ru-Cl	87.83	84.13	82.50	84.40	85.63	85.23	82.67	84.94	82.28

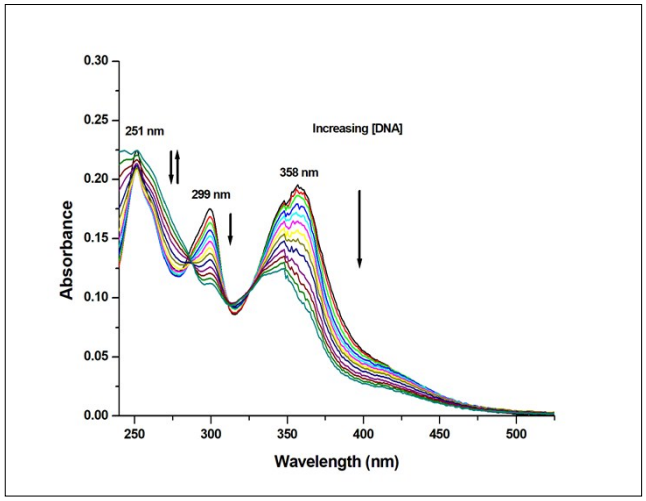

Figure S47. UV-Visible absorption titration spectra of **2** (10 μM; Milli-Q water) with the addition of varying concentrations of CT-DNA (0-15 μM; $T_{10}E_1$ buffer, pH ~ 7.6) at 298 K. UV-Visible absorption spectra of **2** (black).

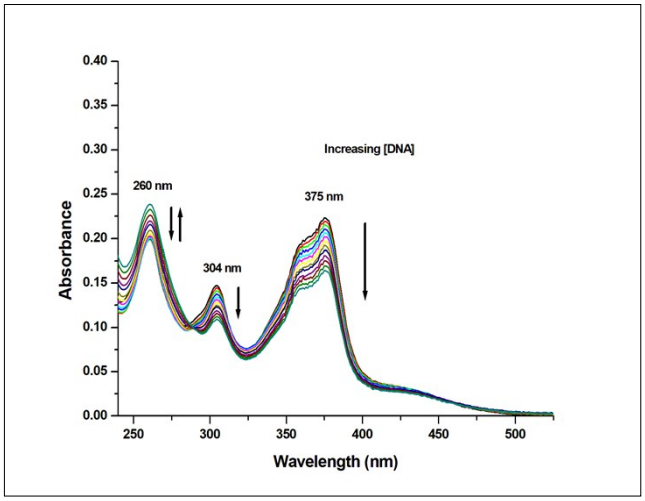

Figure S48. UV-Visible absorption titration spectra of **3** (10 μM; Milli-Q water) with the addition of varying concentrations of CT-DNA (0-15 μM; $T_{10}E_1$ buffer, pH ~ 7.6) at 298 K. UV-Visible absorption spectra of **3** (black).

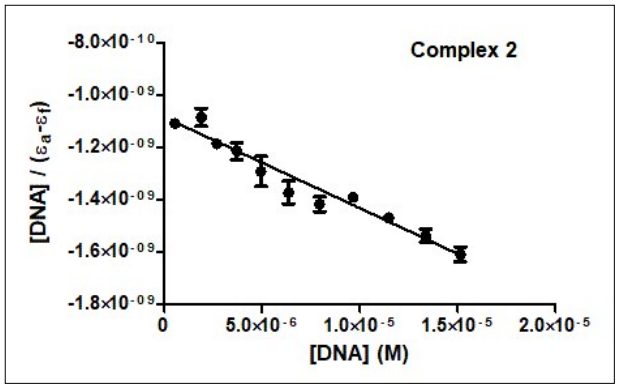

Figure S49. Plot for the calculation of equilibrium binding constant (K_b) associated with the titration of **2** and CT-DNA at 298 K.

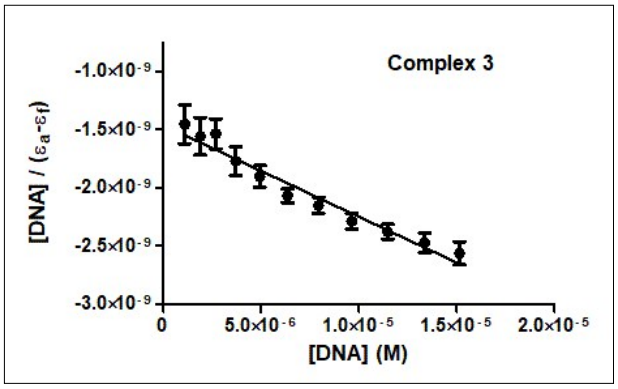

Figure S50. Plot for the calculation of equilibrium binding constant (K_b) associated with the titration of **3** and CT-DNA at 298 K.

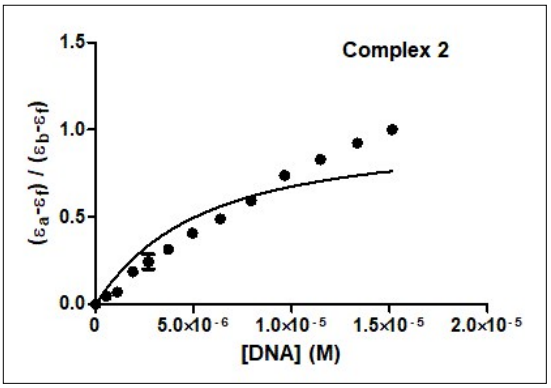

Figure S51. Plot to the model of Bard and Thorp associated with the titration of **2** and CT-DNA at 298 K.

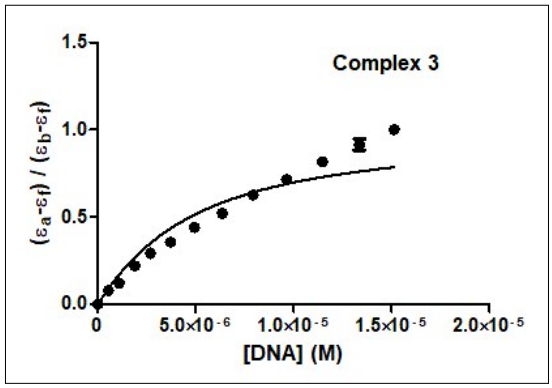

Figure S52. Plot to the model of Bard and Thorp associated with the titration of **3** and CT-DNA at 298 K.

Table S6. Molar absorptivity changes (Δϵ) for UV-Visible absorption studies of DNA binding with complex **1-3**:

Complexes	**Change in molar absorptivity (Δϵ M^{-1} cm^{-1}) and Shift in wavelength (Δλ nm)**			
1	3.47×10^3 hypochromic shift (250 nm)	2.90×10^3 hyper-chromic shift (250 nm)	5.64×10^3 hypochromic shift (301 nm)	7.84×10^3 hypochromic shift (370 nm)
	2 nm (Red Shift)		1 nm (Red Shift)	6 nm (Red Shift)
2	1.64×10^3 hypochromic shift (251 nm)	1.67×10^3 hyper-chromic shift (251 nm)	6.29×10^3 hypochromic shift (299 nm)	9.41×10^3 hypochromic shift (358 nm)
	1 nm (Red Shift)		1 nm (Red Shift)	1 nm (Red Shift)
3	3.99×10^2 hypochromic shift (260 nm)	3.97×10^3 hyper-chromic shift (260 nm)	3.87×10^3 hypochromic shift (304 nm)	5.91×10^3 hypochromic shift (375 nm)
	1 nm (Red Shift)		1 nm (Red Shift)	1 nm (Red Shift)

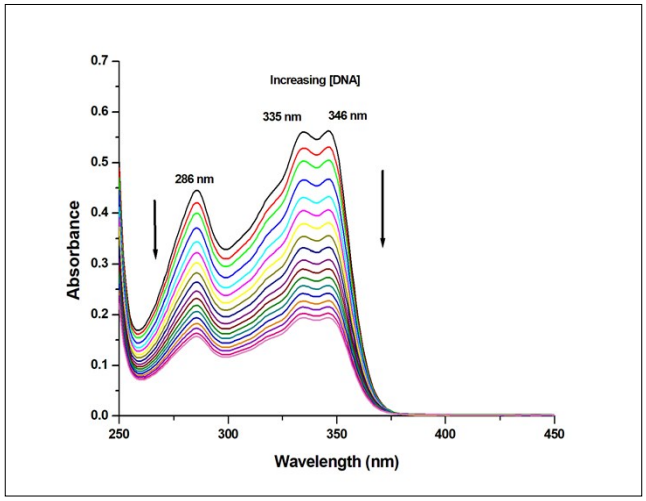

Figure S53. UV-Visible absorption titration spectra of $\mathbf{L_1}$ (25 μM; DMSO:Water (5:100 v/v)) with the addition of varying concentrations of CT-DNA (0-4.3 x 10^{-7} M; $T_{10}E_1$ buffer, pH ~ 7.6) at 298 K. UV-Visible absorption spectra of $\mathbf{L_1}$ (black).

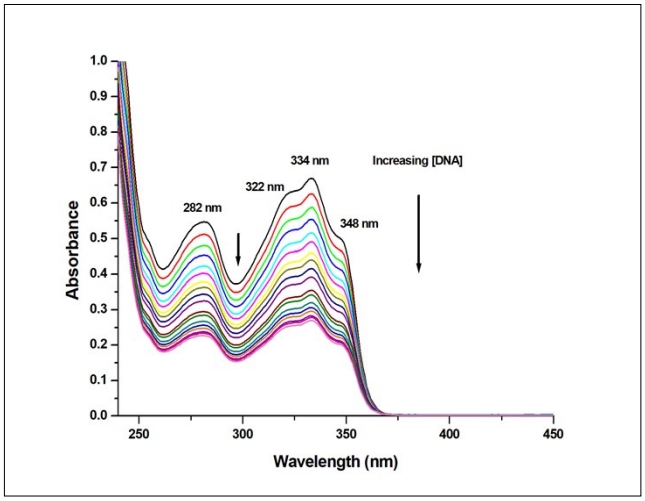

Figure S54. UV-Visible absorption titration spectra of $\mathbf{L_2}$ (25 μM; DMSO:Water (5:100 v/v)) with the addition of varying concentrations of CT-DNA (0-4.3 x 10^{-7} M; $T_{10}E_1$ buffer, pH ~ 7.6) at 298 K. UV-Visible absorption spectra of $\mathbf{L_2}$ (black).

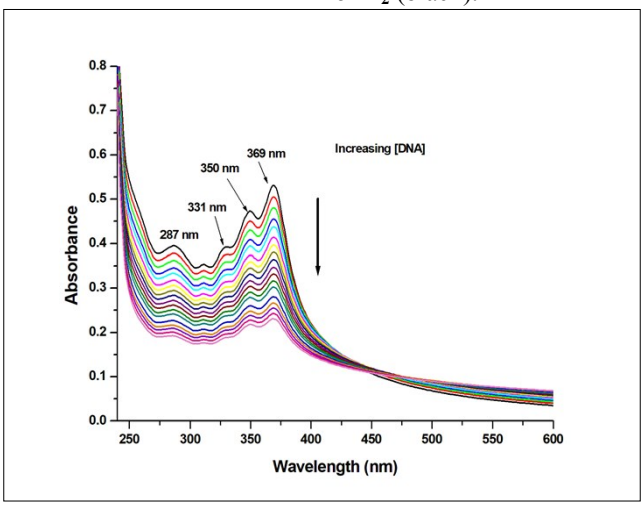

Figure S55. UV-Visible absorption titration spectra of $\mathbf{L_3}$ (25 μM; DMSO:Water (5:100 v/v)) with the addition of varying concentrations of CT-DNA (0-4.3 x 10^{-7} M; $T_{10}E_1$ buffer, pH ~ 7.6) at 298 K. UV-Visible absorption spectra of $\mathbf{L_3}$ (black).

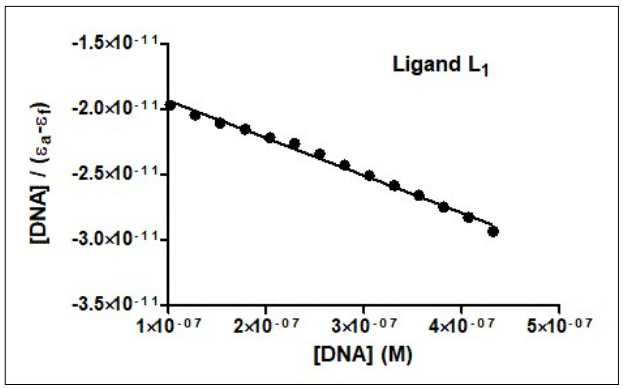

Figure S56. Plot for the calculation of equilibrium binding constant (K_b) associated with the titration of $\mathbf{L_1}$ and CT-DNA at 298 K.

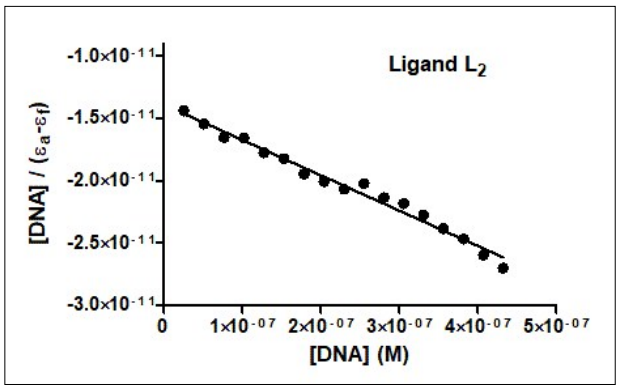

Figure S57. Plot for the calculation of equilibrium binding constant (K_b) associated with the titration of $\mathbf{L_2}$ and CT-DNA at 298 K.

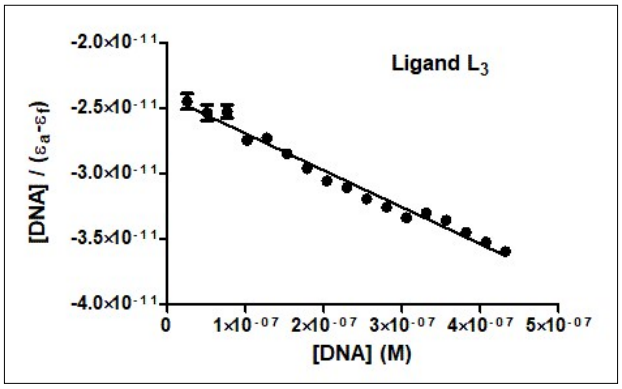

Figure S58. Plot for the calculation of equilibrium binding constant (K_b) associated with the titration of $\mathbf{L_3}$ and CT-DNA at 298 K.

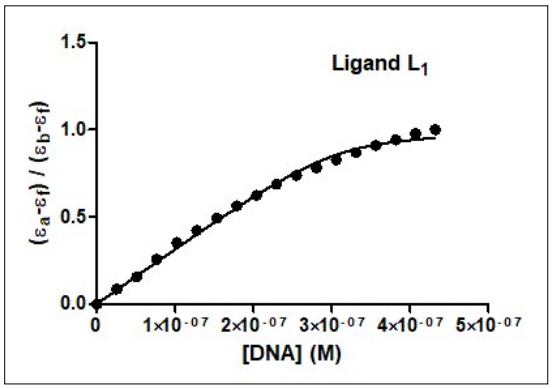

Figure S59. Plot to the model of Bard and Thorp associated with the titration of $\mathbf{L_1}$ and CT-DNA at 298 K.

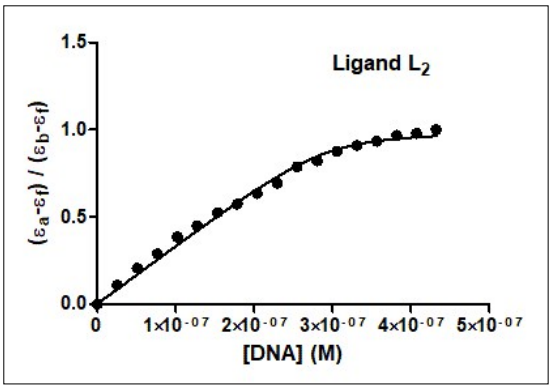

Figure S60. Plot to the model of Bard and Thorp associated with the titration of $\mathbf{L_2}$ and CT-DNA at 298 K.

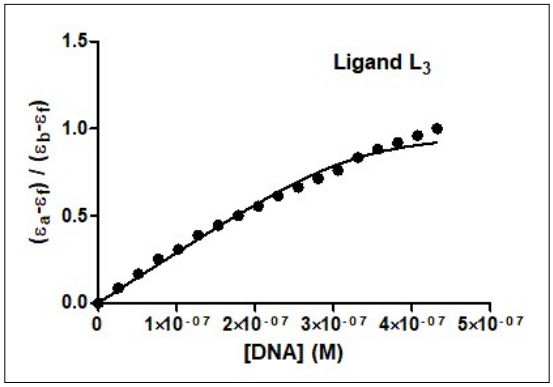

Figure S61. Plot to the model of Bard and Thorp associated with the titration of $\mathbf{L_3}$ and CT-DNA at 298 K.

Table S7. Data for UV-Visible absorption studies for DNA binding with ligand L_1-L_3:

Compounds	Equilibrium Binding Constant (K_b) (in M^{-1})	Binding site size (s) (per base pair)
Ligand L_1	$1.73 \pm 0.03 \times 10^6$	0.0061
Ligand L_2	$2.04 \pm 0.03 \times 10^6$	0.0058
Ligand L_3	$1.16 \pm 0.02 \times 10^6$	0.0065

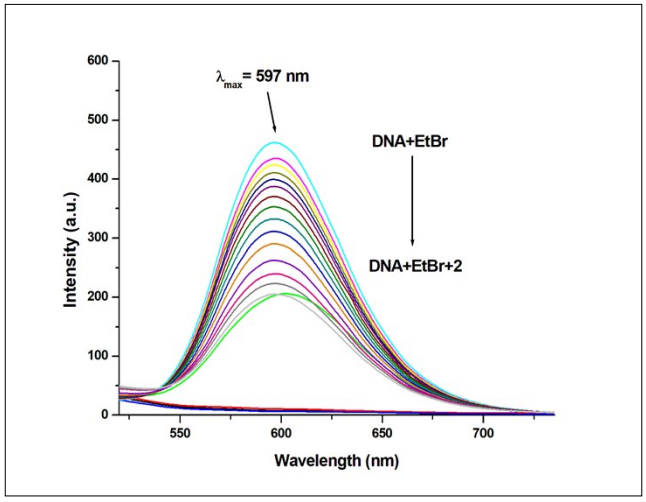

Figure S62. Molecular fluorescence emission profile associated with titration of EthBr-DNA (35 μM; $T_{10}E_1$ buffer, pH ~ 7.6; $\lambda_{ex.}$ 480 nm; $\lambda_{em.}$ 597 nm) with the addition of varying concentrations of **2** (0-360 μM; Milli-Q water) at 298 K. Fluorescence spectra of only buffer (black), only DNA (red) and only EthBr (green) only **2** (blue) and EthBr-DNA(cyan).

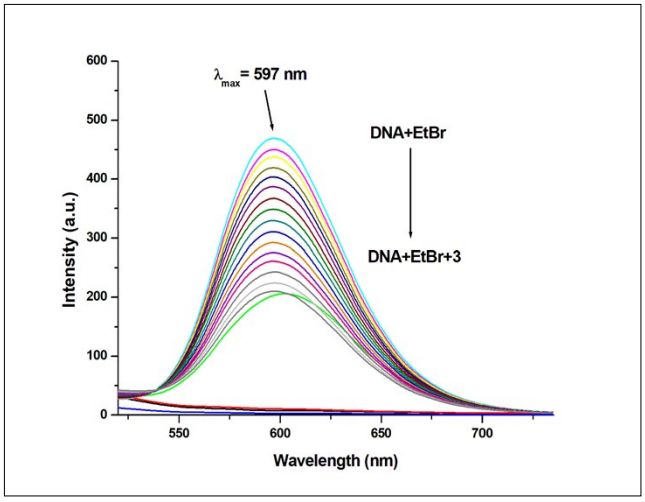

Figure S63. Molecular fluorescence emission profile associated with titration of EthBr-DNA (35 μM; $T_{10}E_1$ buffer, pH ~ 7.6; $\lambda_{ex.}$ 480 nm; $\lambda_{em.}$ 597 nm) with the addition of varying concentrations of **3** (0-270 μM; Milli-Q water) at 298 K. Fluorescence spectra of only buffer (black), only DNA (red) and only EthBr (green) only **3** (blue) and EthBr-DNA(cyan).

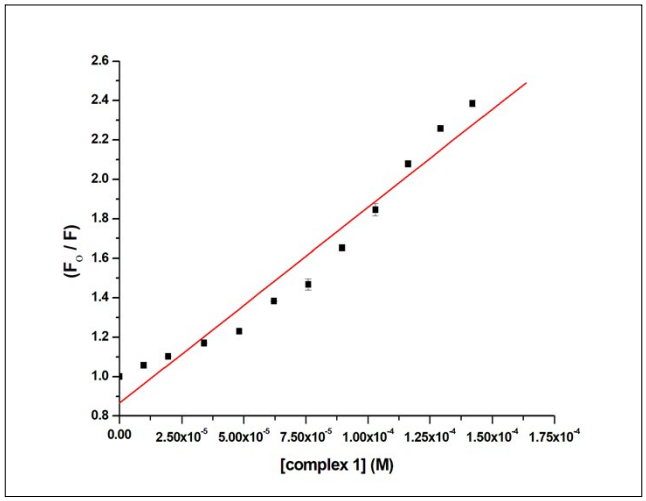

Figure S64. Stern-Volmer plot for the calculation of quenching constant (K_{SV}) associated with the titration of EthBr-DNA and **1** at 298 K.

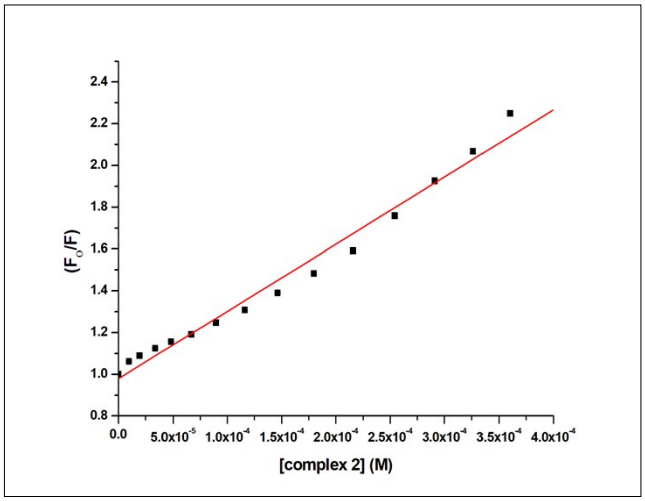

Figure S65. Stern-Volmer plot for the calculation of quenching constant (K_{SV}) associated with the titration of EthBr-DNA and **2** at 298 K.

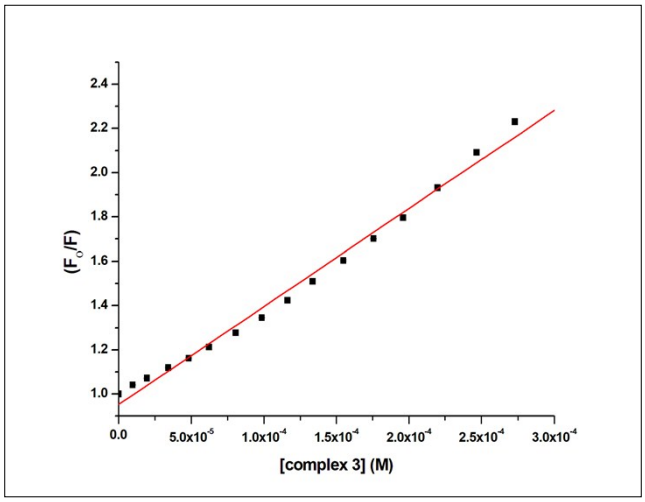

Figure S66. Stern-Volmer plot for the calculation of quenching constant (K_{SV}) associated with the titration of EthBr-DNA and **3** at 298 K.

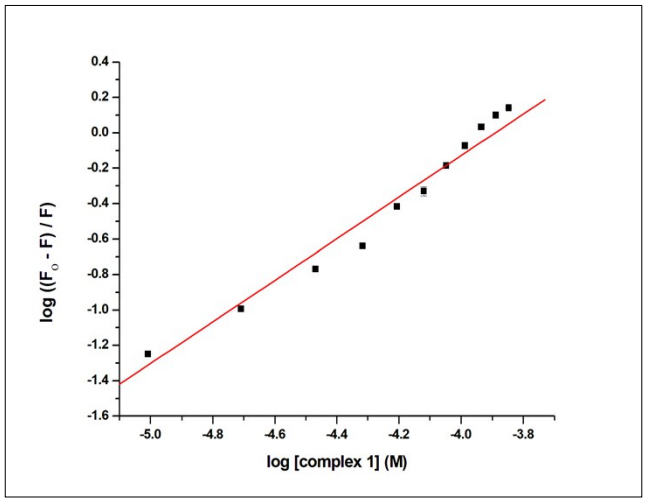

Figure S67. Scatchard plot for the calculation of association constant (K_a) related with the interaction of EthBr-DNA and **1** at 298 K.

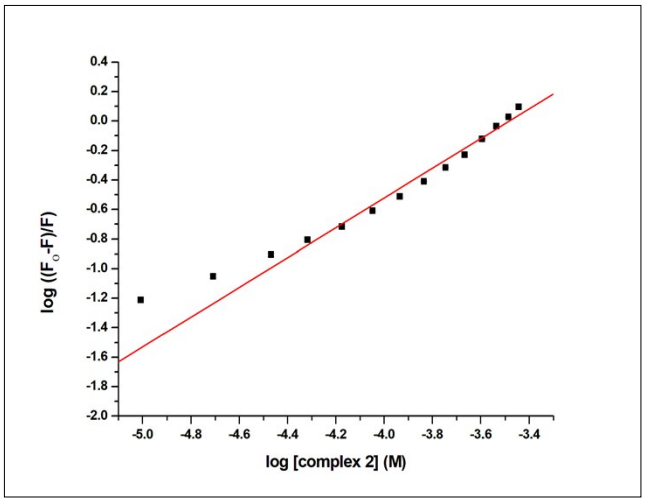

Figure S68. Scatchard plot for the calculation of association constant (K_a) related with the interaction of EthBr-DNA and **2** at 298 K.

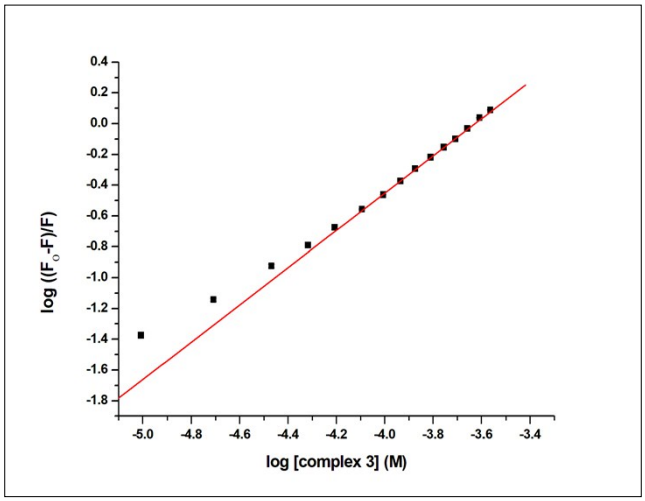

Figure S69. Scatchard plot for the calculation of association constant (K_a) related with the interaction of EthBr-DNA and **3** at 298 K.

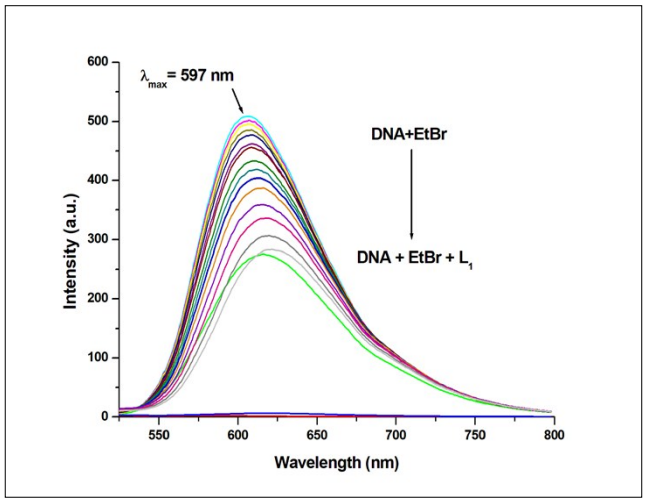

Figure S70. Molecular fluorescence emission profile associated with titration of EthBr-DNA (35 μM; $T_{10}E_1$ buffer, pH ~ 7.6; $\lambda_{ex.}$ 480 nm; $\lambda_{em.}$ 597 nm) with the addition of varying concentrations of $\mathbf{L_1}$ (0-7.24 x 10^{-4} M; DMSO:Water (5:100 v/v)) at 298 K. Fluorescence spectra of only buffer (black), only DNA (red) and only EthBr (green) only **2** (blue) and EthBr-DNA(cyan).

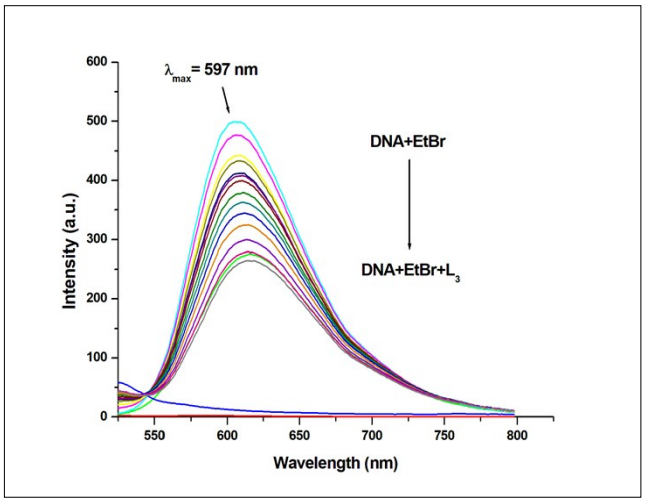

Figure S71. Molecular fluorescence emission profile associated with titration of EthBr-DNA (35 μM; $T_{10}E_1$ buffer, pH ~ 7.6; $\lambda_{ex.}$ 480 nm; $\lambda_{em.}$ 597 nm) with the addition of varying concentrations of $\mathbf{L_3}$ (0-4.42 x 10^{-4} M ; DMSO:Water (5:100 v/v)) at 298 K. Fluorescence spectra of only buffer (black), only DNA (red) and only EthBr (green) only **2** (blue) and EthBr-DNA(cyan).

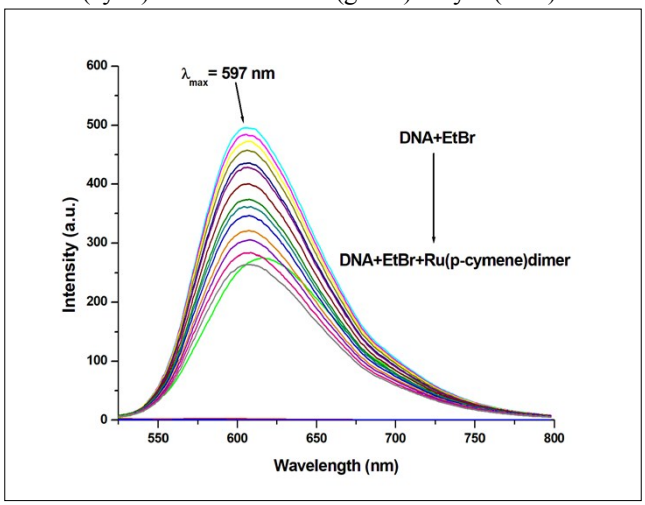

Figure S72. Molecular fluorescence emission profile associated with titration of EthBr-DNA (35 μM; $T_{10}E_1$ buffer, pH ~ 7.6; $\lambda_{ex.}$ 480 nm; $\lambda_{em.}$ 597 nm) with the addition of varying concentrations of Ru(p-cymene)dimer (0-6.03 x 10^{-4} M; Milli-Q water) at 298 K. Fluorescence spectra of only buffer (black), only DNA (red) and only EthBr (green) only **2** (blue) and EthBr-DNA(cyan).

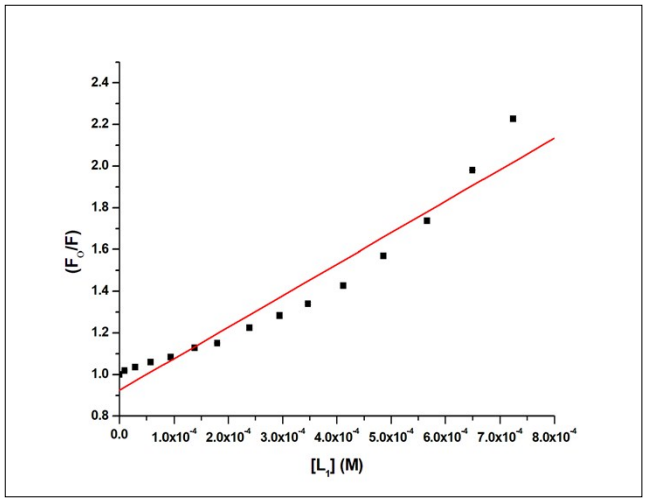

Figure S73. Stern-Volmer plot for the calculation of quenching constant (K_{SV}) associated with the titration of EthBr-DNA and $\mathbf{L_1}$ at 298 K.

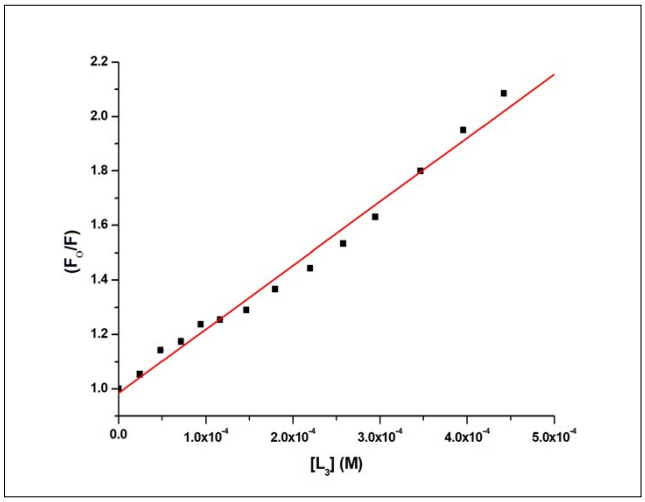

Figure S74. Stern-Volmer plot for the calculation of quenching constant (K_{SV}) associated with the titration of EthBr-DNA and $\mathbf{L_3}$ at 298 K.

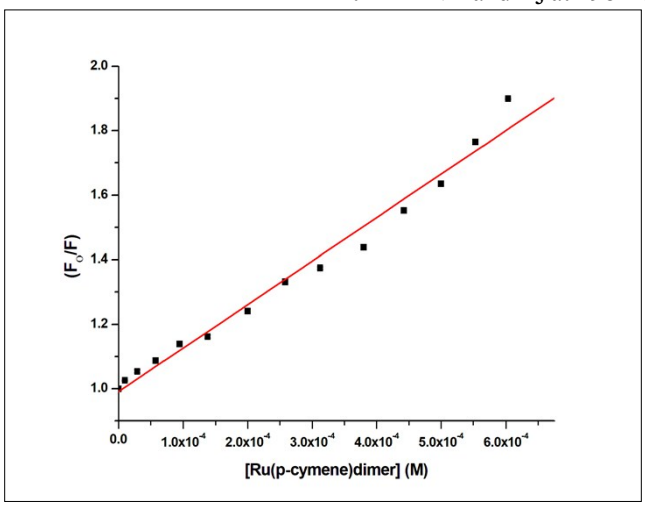

Figure S75. Stern-Volmer plot for the calculation of quenching constant (K_{SV}) associated with the titration of EthBr-DNA and Ru(p-cymene)dimer at 298 K.

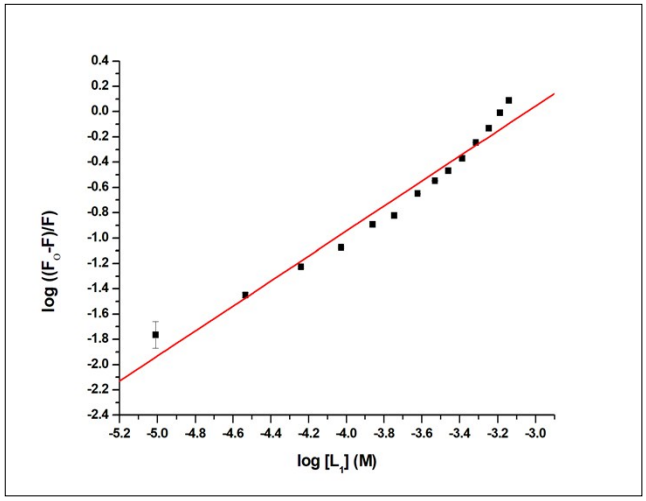

Figure S76. Scatchard plot for the calculation of association constant (K_a) related with the interaction of EthBr-DNA and $\mathbf{L_1}$ at 298 K.

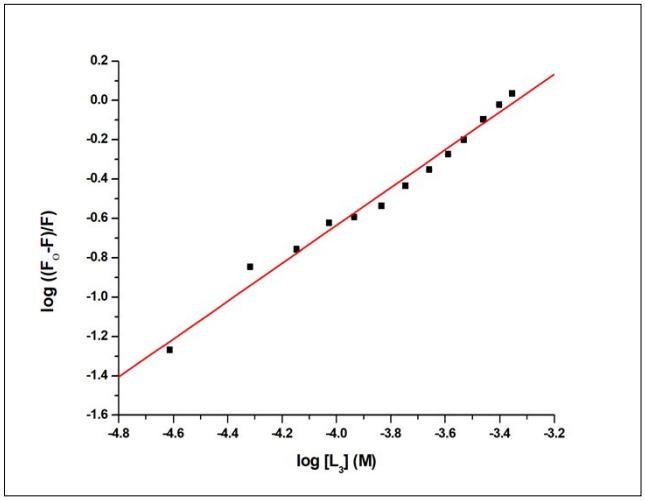

Figure S77. Scatchard plot for the calculation of association constant (K_a) related with the interaction of EthBr-DNA and $\mathbf{L_3}$ at 298 K.

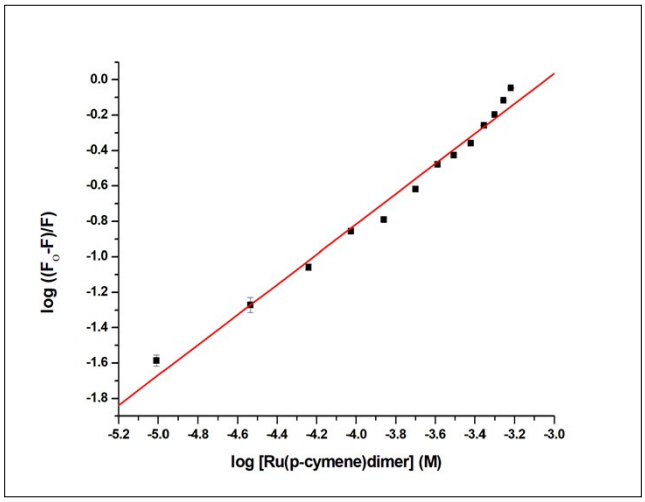

Figure S78. Scatchard plot for the calculation of association constant (K_a) related with the interaction of EthBr-DNA and Ru(p-cymene)dimer at 298 K.

Table S8. Data for emission spectroscopic studies for DNA binding with ligand $\mathbf{L_1}$, $\mathbf{L_3}$ and Ru(p-cymene)dimer:

Compounds	**Quenching constant (K_{SV}) (M^{-1})**	**Association Constant (K_a)(M^{-1})**	**No. of binding site (n)**
Ligand $\mathbf{L_1}$	$1.51 \pm 0.023 \times 10^3$	$1.10 \pm 0.32 \times 10^3$	0.98
Ligand $\mathbf{L_3}$	$2.34 \pm 0.033 \times 10^3$	$1.62 \pm 0.06 \times 10^3$	0.96
Ru(p-cymene)dimer	$1.35 \pm 0.027 \times 10^3$	$4.01 \pm 0.67 \times 10^2$	0.85

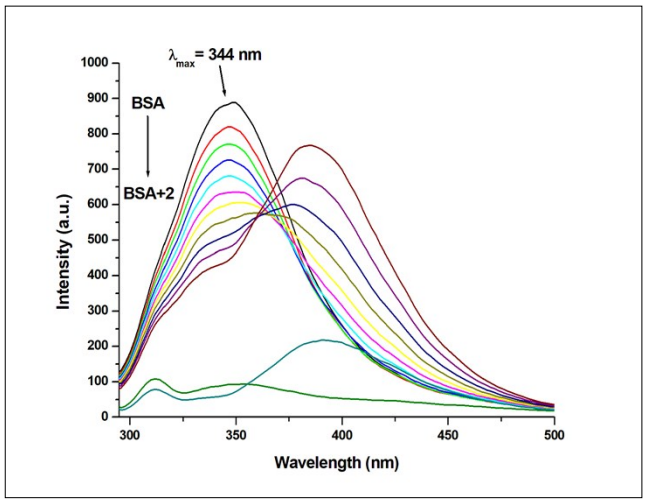

Figure S79. Molecular fluorescence emission profile associated with titration of BSA (0.15 µM; PBS, pH ~ 7.4; $\lambda_{ex.}$ 280 nm; $\lambda_{em.}$ 344 nm) with the addition of varying concentrations of **2** (0-16 µM; PBS, pH ~ 7.4) at 298 K. Fluorescence spectra of BSA (black), only buffer (dark green) and only complex (ocean blue).

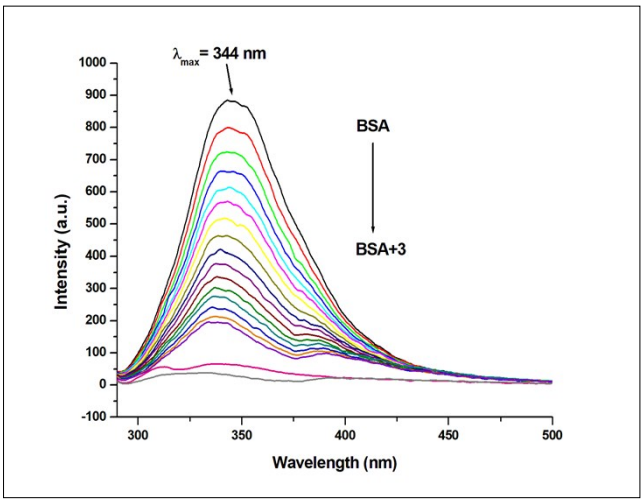

Figure S80. Molecular fluorescence emission profile associated with titration of BSA (0.15 µM; PBS, pH ~ 7.4; $\lambda_{ex.}$ 280 nm; $\lambda_{em.}$ 344 nm) with the addition of varying concentrations of **3** (0-16 µM; PBS, pH ~ 7.4) at 298 K. Fluorescence spectra of BSA (black), only buffer (pink) and only complex (grey).

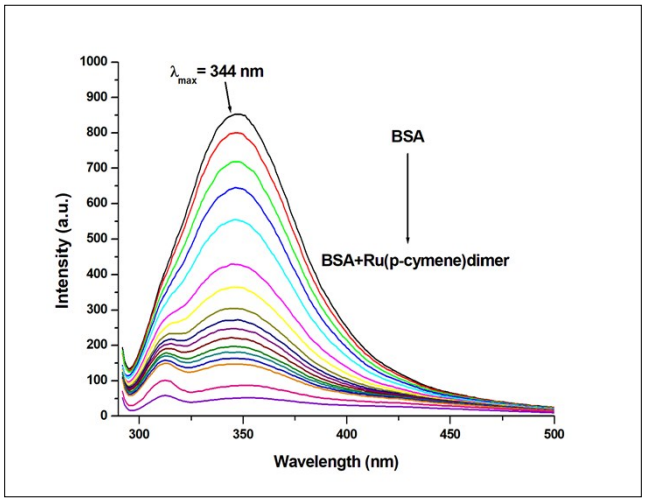

Figure S81. Molecular fluorescence emission profile associated with titration of BSA (0.15 μM; PBS, pH ~ 7.4; $\lambda_{ex.}$ 280 nm; $\lambda_{em.}$ 344 nm) with the addition of varying concentrations of Ru(p-cymene)dimer (0-16 μM; PBS, pH ~ 7.4) at 298 K. Fluorescence spectra of BSA (black), only buffer (purple) and only complex (pink).

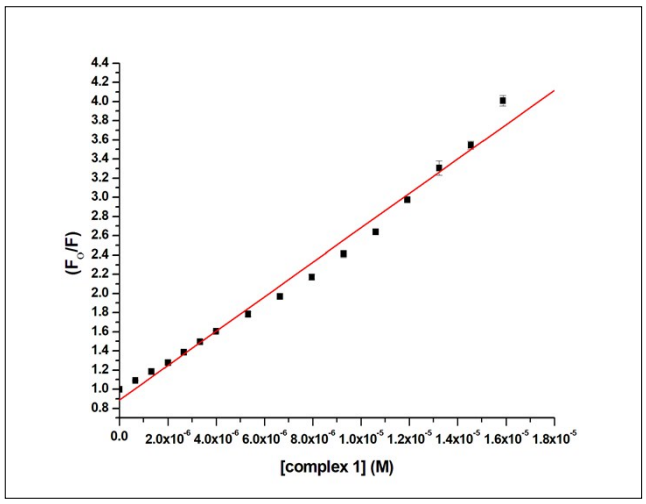

Figure S82. Stern-Volmer plot for the calculation of quenching constant (K_{SV}) associated with the interaction of BSA and **1** at 298 K.

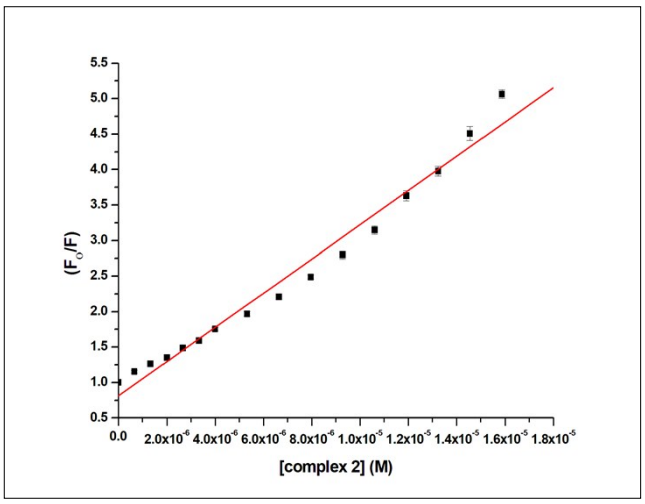

Figure S83. Stern-Volmer plot for the calculation of quenching constant (K_{SV}) associated with the interaction of BSA and **2** at 298 K.

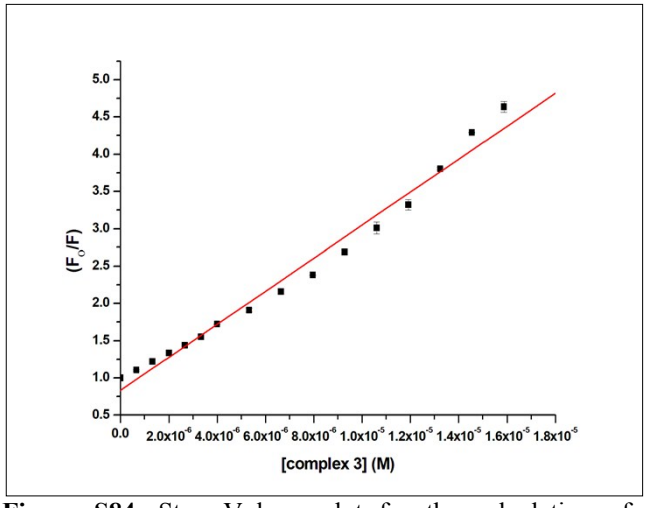

Figure S84. Stern-Volmer plot for the calculation of quenching constant (K_{SV}) associated with the interaction of BSA and **3** at 298 K.

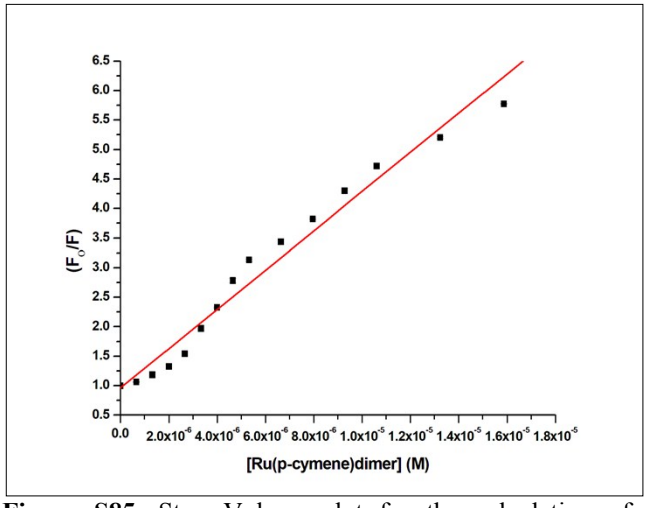

Figure S85. Stern-Volmer plot for the calculation of quenching constant (K_{SV}) associated with the interaction of BSA and Ru(p-cymene)dimer at 298 K.

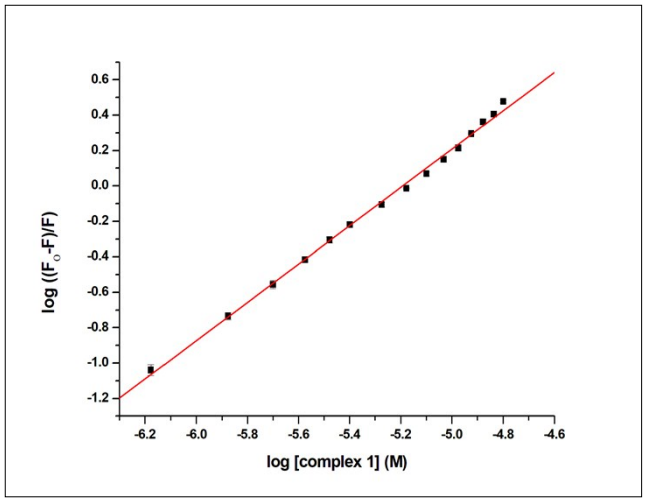

Figure S86. Scatchard plot for the calculation of binding constant (K_b) associated with the interaction of BSA and **1** at 298 K.

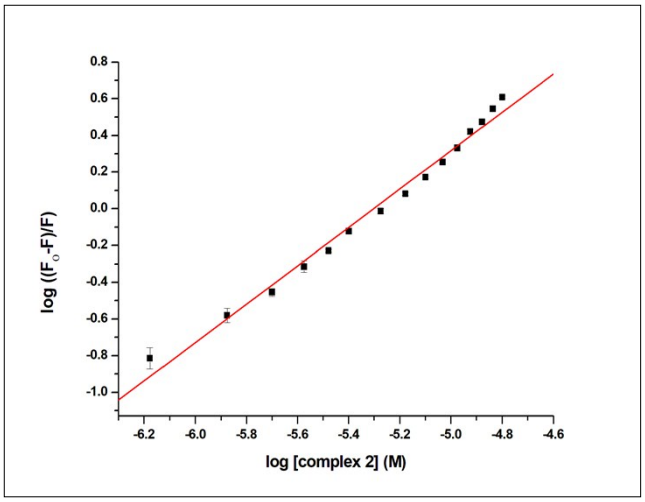

Figure S87. Scatchard plot for the calculation of binding constant (K_b) associated with the interaction of BSA and **2** at 298 K.

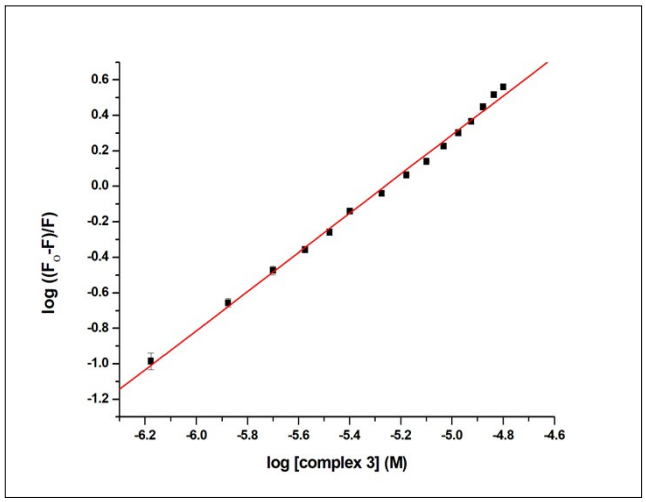

Figure S88. Scatchard plot for the calculation of binding constant (K_b) associated with the interaction of BSA and **3** at 298 K.

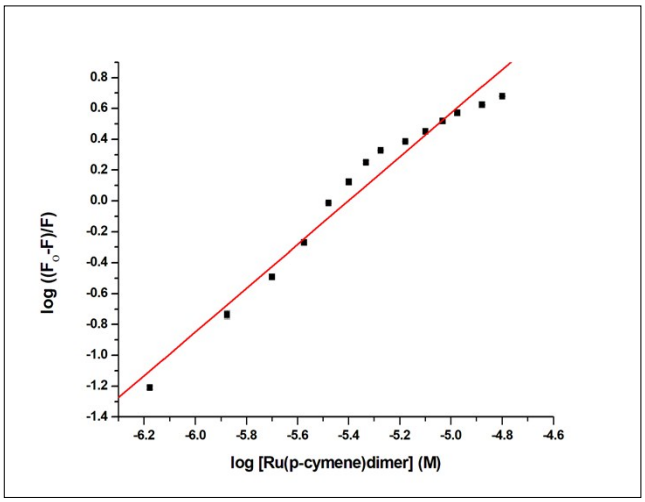

Figure S89. Scatchard plot for the calculation of binding constant (K_b) associated with the interaction of BSA and Ru(p-cymene)dimer at 298 K.

Table S9. Data for emission spectroscopic studies for BSA interaction with Ru(p-cymene)dimer:

Complex	**Quenching constant (K_{SV}) (M^{-1})**	**Binding Constant (K_b)(M^{-1})**	**No. of binding site (n)**
Ru(p-cymene)dimer	$3.32 \pm 0.099 \times 10^5$	$4.73 \pm 0.84 \times 10^7$	1.42

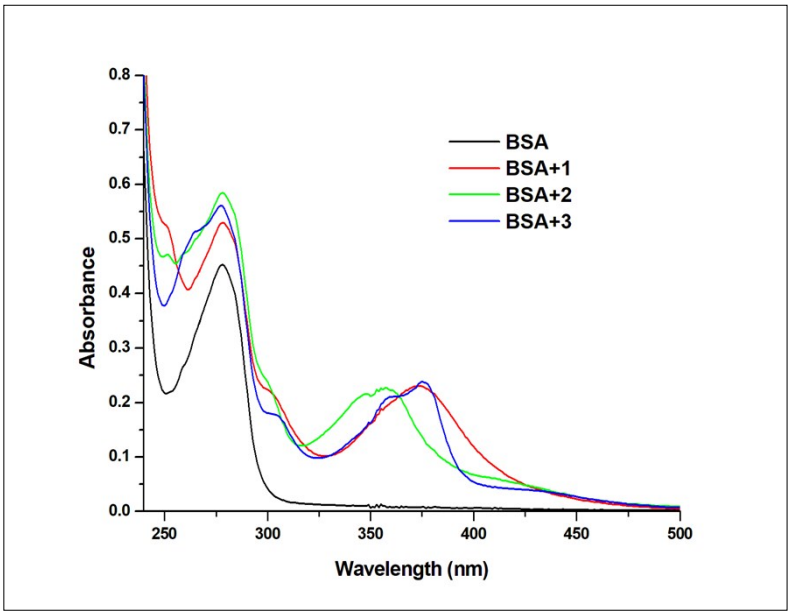

Figure S90. UV-Visible absorption spectra of BSA (10 μM; PBS, pH ~ 7.4) in presence of **1-3** (10 μM; PBS, pH ~ 7.4) at 298 K.

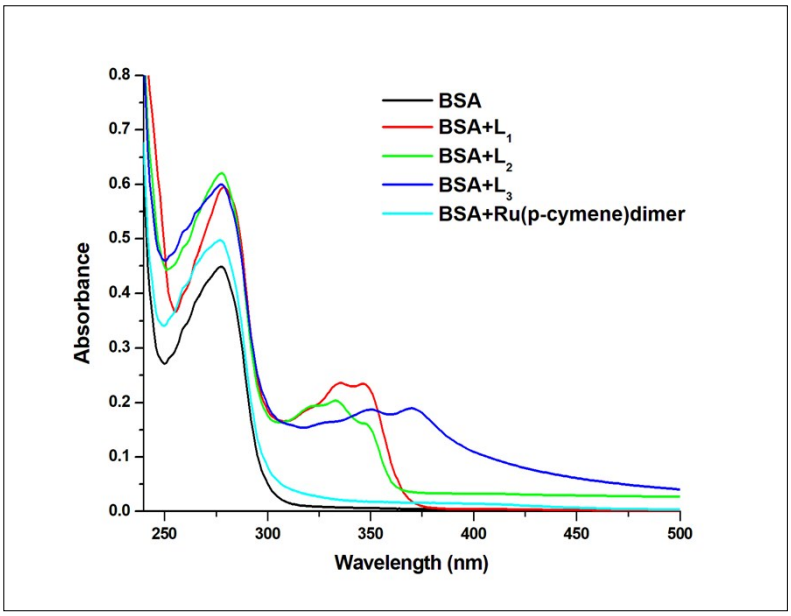

Figure S91. UV-Visible absorption spectra of BSA (10 μM; PBS, pH ~ 7.4) in presence of $\mathbf{L_1}$, $\mathbf{L_2}$, $\mathbf{L_3}$ and Ru(p-cymene)dimer (10 μM; DMSO:Water (5:100 v/v)) at 298 K.

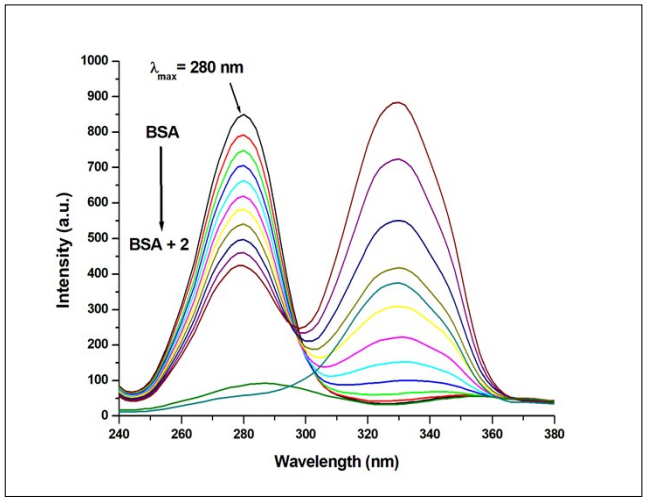

Figure S92. Synchronous fluorescence emission profile associated with titration of BSA (0.15 μM; PBS, pH ~ 7.4) with the addition of varying concentrations of **2** (0-16 μM; PBS, pH ~ 7.4) at the wavelength difference of Δλ = 60 nm. Fluorescence spectra of BSA (black), only buffer (dark green) and only complex (ocean blue).

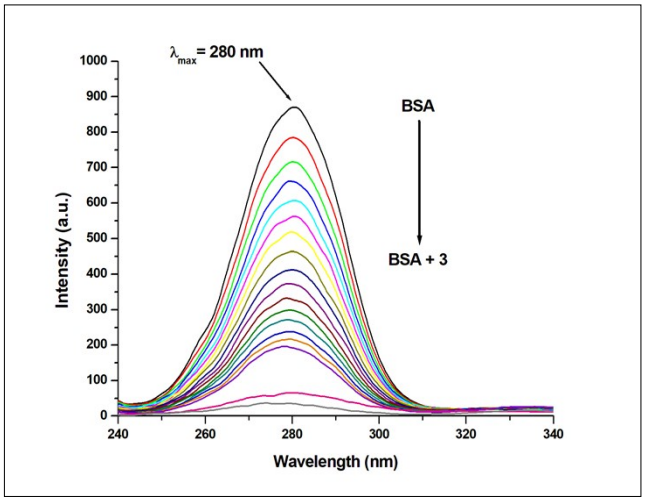

Figure S93. Synchronous fluorescence emission profile associated with titration of BSA (0.15 μM; PBS, pH ~ 7.4) with the addition of varying concentrations of **3** (0-16 μM; PBS, pH ~ 7.4) at the wavelength difference of Δλ = 60 nm. Fluorescence spectra of BSA (black), only buffer (pink) and only complex (grey).

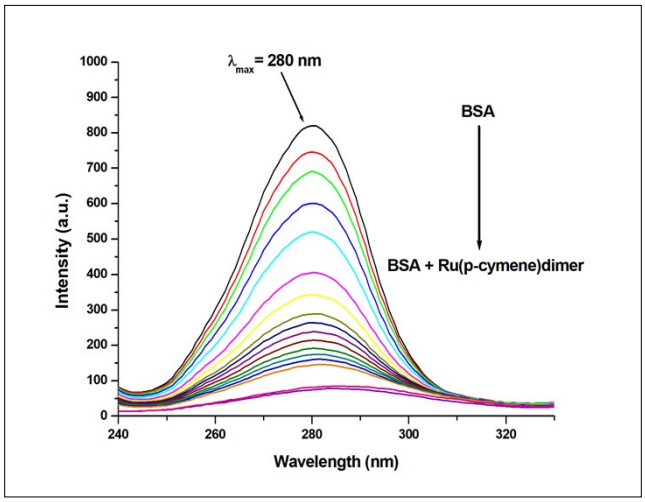

Figure S94. Synchronous fluorescence emission profile associated with titration of BSA (0.15 μM; PBS, pH ~ 7.4) with the addition of varying concentrations of Ru(p-cymene)dimer (0-16 μM; PBS, pH ~ 7.4) at the wavelength difference of Δλ = 60 nm. Fluorescence spectra of BSA (black), only buffer (purple) and only complex (pink).

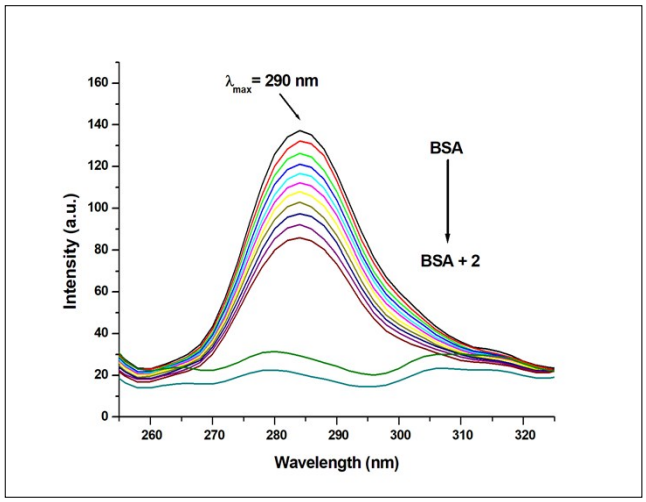

Figure S95. Synchronous fluorescence emission profile associated with titration of BSA (0.15 μM; PBS, pH ~ 7.4) with the addition of varying concentrations of **2** (0-16 μM; PBS, pH ~ 7.4) at the wavelength difference of Δλ = 15 nm. Fluorescence spectra of BSA (black), only buffer (dark green) and only complex (ocean blue).

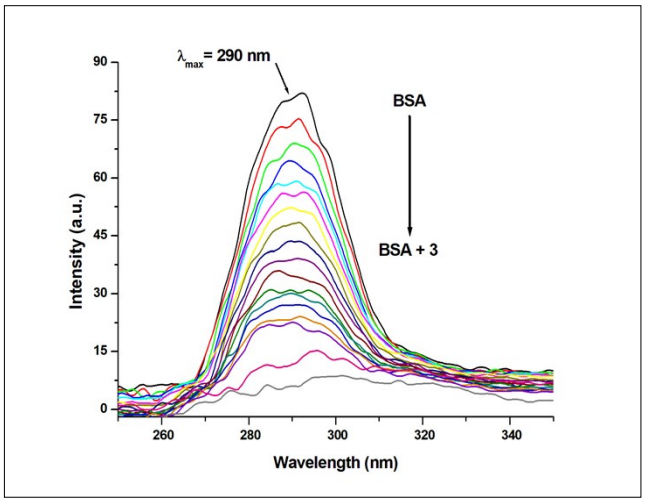

Figure S96. Synchronous fluorescence emission profile associated with titration of BSA (0.15 μM; PBS, pH ~ 7.4) with the addition of varying concentrations of **3** (0-16 μM; PBS, pH ~ 7.4) at the wavelength difference of Δλ = 15 nm. Fluorescence spectra of BSA (black), only buffer (pink) and only complex (grey).

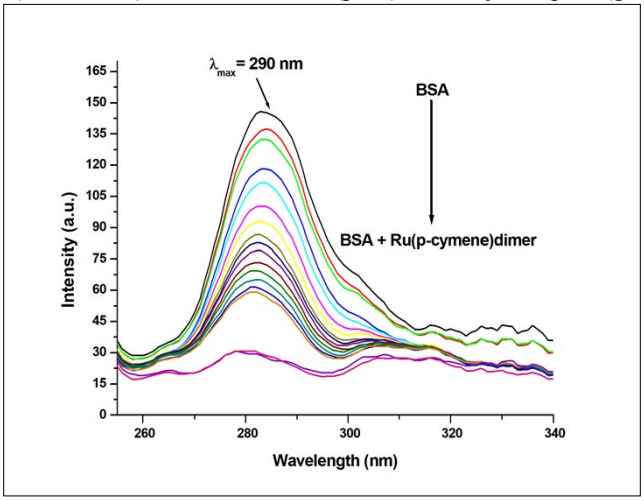

Figure S97. Synchronous fluorescence emission profile associated with titration of BSA (0.15 μM; PBS, pH ~ 7.4) with the addition of varying concentrations of Ru(p-cymene)dimer (0-16 μM; PBS, pH ~ 7.4) at the wavelength difference of Δλ = 15 nm. Fluorescence spectra of BSA (black), only buffer (purple) and only complex (pink).

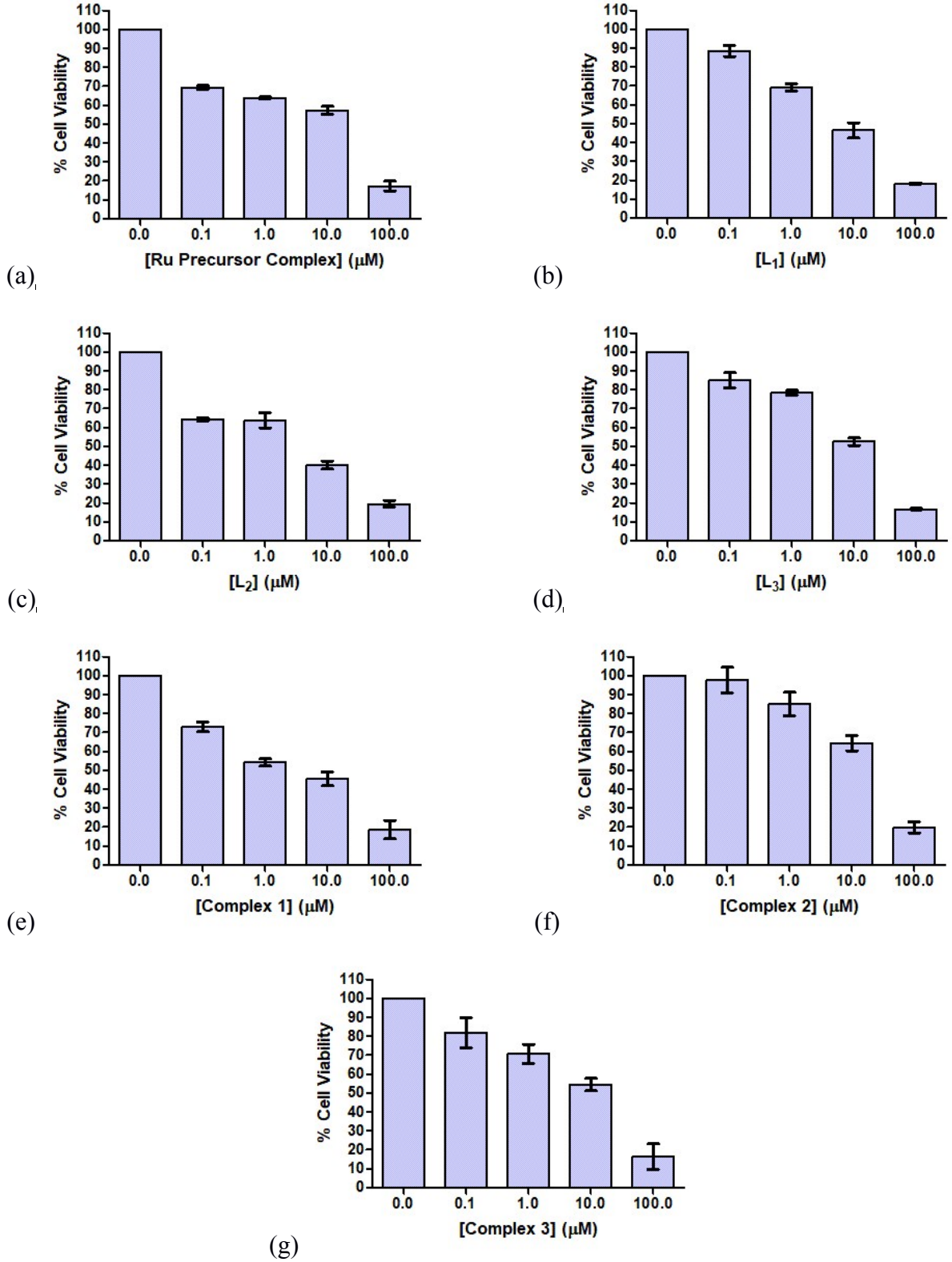

Figure S98. *In vitro* cytotoxicity of **Ru precursor complex** (a), $\mathbf{L_1}$ (b), $\mathbf{L_2}$ (c), $\mathbf{L_3}$ (d), complex **1** (e), complex **2** (f) and complex **3** (g) against MCF-7 cell lines measured by MTT assay after 48 h.

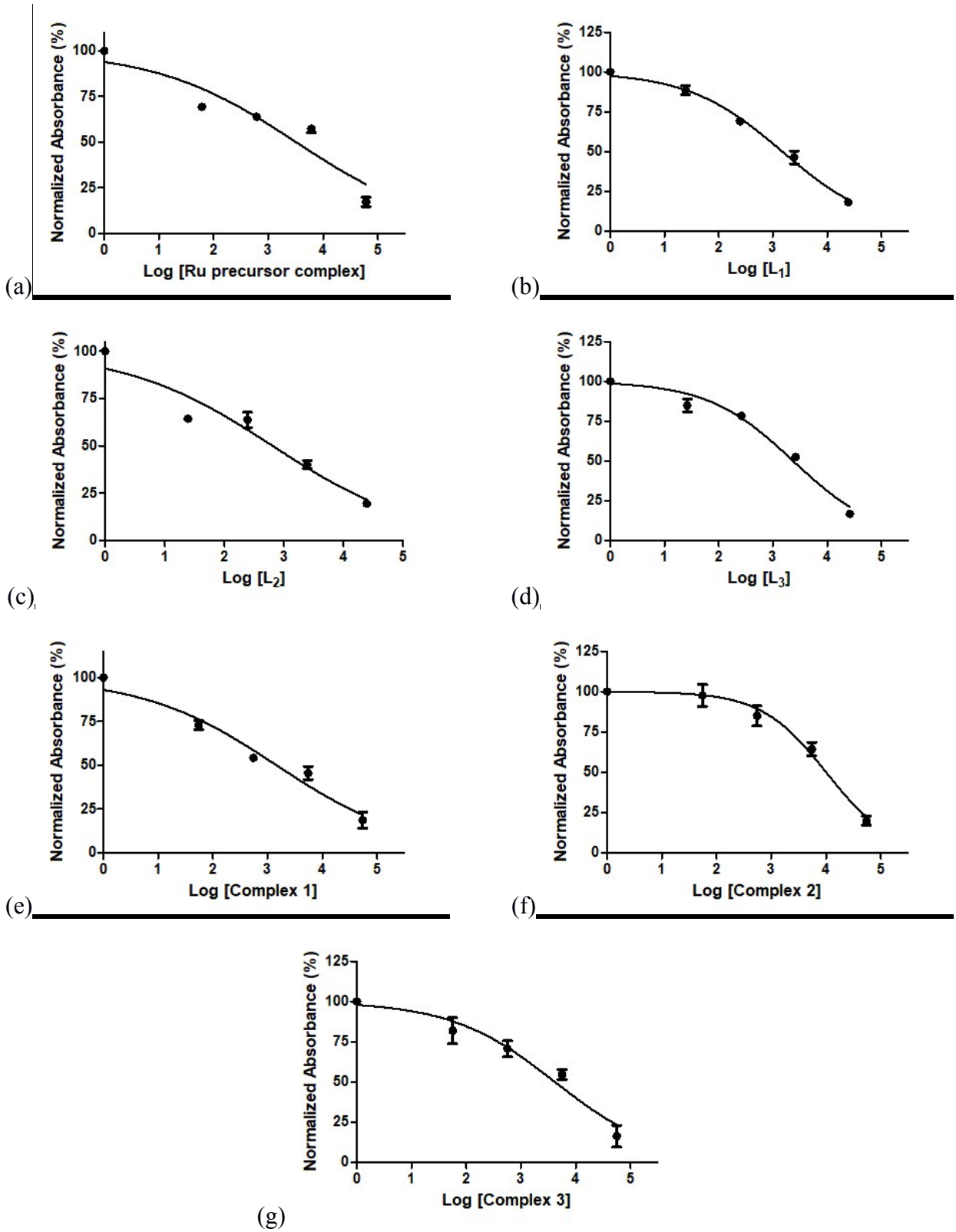

Figure S99. *In vitro* calculated IC_{50} values of **Ru precursor complex** (a), $\mathbf{L_1}$ (b), $\mathbf{L_2}$ (c), $\mathbf{L_3}$ (d), complex **1** (e), complex **2** (f) and complex **3** (g) against MCF-7 cell lines measured by MTT assay after 48 h.

Reference:

(1) Kumar, A.; Kumar, A.; Gupta, R. K.; Paitandi, R. P.; Singh, K. B.; Trigun, S. K.; Hundal, M. S.; Pandey, D. S. *Journal of Organometallic Chemistry* **2016**, *801*, 68.